Journal of Structural Geology 191 (2025) 105288

Contents lists available at ScienceDirect

Journal of Structural Geology

journal homepage: www.elsevier.com/locate/jsg

Morphotectonics, slope stability and paleostress studies from the Bhagirathi river section, western Himalaya (Uttarakhand, India)

Nikhil Puniya [a], Soumyajit Mukherjee [b,*], Atul Kumar Patidar [a,**], Mohit Kumar Puniya [c], Mery Biswas [d], Tuhin Biswas [e]

[a] Department of Petroleum Engineering & Earth Sciences, UPES, Dehradun, 248 007, Uttarakhand, India
[b] Department of Earth Sciences, Indian Institute of Technology Bombay Powai, Mumbai, 400 076, Maharashtra, India
[c] Uttarakhand Landslide Mitigation and Management Centre, Disaster Authority of Uttarakhand, Dehradun, 248 001, Uttarakhand, India
[d] Department of Geography, Presidency University, Kolkata, West Bengal, 700 073, India
[e] 1010 Rocky Rd Socorro, New Mexico, USA

ARTICLE INFO

Keywords:
Morphometry
Landslides
Slope stability
Paleostress analysis
Collisional tectonics

ABSTRACT

We study parts of Tethyan, Higher and Lesser Himalayan rocks along the Bhagirathi river valley for morphotectonic analysis. The spatial and linear properties of the 21 sub-watersheds (S-WSs) and the Bhagirathi main watershed provide strong evidence of active tectonics mainly in the S-WS 3 (through which the South Tibetan Detachment passes), S-WS 9 (no fault runs), S-WS 12 (Vaikrita, Munsiari and Tons Thrusts cross) and S-WS 17 (Basul and Tons Thrusts occur). The Technique for Order Preference by Similarity to Ideal Solution (TOPSIS) has been used to classify the sub-watersheds as per the intensity of their recent tectonic activity. Seven morphometric parameters are used for the TOPSIS analysis. From the Lesser Himalayan section additionally, we perform landslide and paleostress studies. Eleven slopes cuts and 24 landslides were investigated to determine the mode of failure in a portion of the Rishikesh-Gangotri Highway. Landslides in soil strata is caused mainly by the low cohesion and due to the presence of coarse-grained loose materials. In the present study, most landslides (and earthquakes) have occurred in the vicinity of major thrusts. Where there is a high frequency of slickenside related to brittle normal faulting (K2 zone, near Dunda, Singuni and Dharasu Thrusts), a higher earthquake frequency of 3.5–5.2 magnitude is observed from the data set of around last 75 years. Paleostress analysis on data-sets of normal, reverse and strike-slip movements using the WinTensor software (ver. 5.8.8) yields NNE-SSW direction of extension for normal slip, NE-SW compression for reverse movement, and a pure strike-slip tensor with NNE-SSW shortening and WWN-SSE direction of maximum extension. The K2 zone where these deformations were most documented is also the place of slope instability and high present-day tectonic activity.

1. Introduction

Geohazards in collisional orogens, especially in the (western) Himalaya, have received wide attention in recent years (e.g., Jayangondaperumal et al., 2018; Kumar et al., 2023). The Himalayan collisional orogen started developing from ~ 55 Ma when continent-continent collision between the Eurasian and the Indian plates took place (Yin, 2006) and produced non-planar triclinic transpression (Dutta and Mukherjee, 2021). The Himalayan orogen consists of, towards north, the Sub-Himalaya (SH) dominantly of sedimentary rocks; Proterozoic phyllites, slates, schists and gneisses of the Lesser Himalaya (LH); higher-grade schists and gneisses of the Higher Himalaya (HH); and Paleozoic Mesozoic marine sediments of the Tethyan Himalaya (TH). Main Boundary Thrust (MBT), Main Central Thrust (MCT) and South Tibetan Detachment (STD) are the southern boundaries of the LH, HH and TH, respectively (review in Mukherjee, 2013, 2015a). The LH is bound by ~ N/NE -dipping MBT at south (Bose and Mukherjee, 2020) and the Main Central Thrust at north (Bose and Mukherjee, 2019). From the MCT at north up to the Tons Thrust (TT) (/Srinagar Thrust/Almora Thrust) at south in the Garhwal region (India) is called as the Inner Lesser Himalaya (ILH). The entire LH has been a matter of international attention for tectonics, stratigraphy and resource issues (e.g., Biswas

* Corresponding author.
** Corresponding author.
E-mail addresses: smukherjee@iitb.ac.in, soumyajitm@gmail.com (S. Mukherjee), apatidar@ddn.upes.ac.in, atulpatidar@gmail.com (A.K. Patidar).

https://doi.org/10.1016/j.jsg.2024.105288
Received 19 August 2024; Received in revised form 23 October 2024; Accepted 6 November 2024
Available online 26 November 2024

et al., 2022). Being a part of an active mountain belt, LH is characterized by geohazards e.g., earthquakes, landslides and flash floods (e.g., Kanga et al., 2022).

Morphology of drainage basins can indicate recent tectonics (Barman et al., 2020; Choudhari et al., 2018; Dasgupta et al., 2023). The utilization of remote-sensing platforms and Geographical Information System (GIS) enable the calculation of morphometric indices, facilitating comprehensive analysis of heterogeneous geographic datasets (Remondo and Oguchi, 2009). These methodologies have facilitated the quantitative assessment of geomorphic features and their accurate representation across various spatial scales, notably in the context of river basin analyses (Evans et al., 2009; Pike et al., 2009).

Recently there has been a notable surge in the utilizing multi-criteria decision-making (MCDM) models for assessing recent tectonics of terrains. For this purpose, TOPSIS model has been in use (review in Table 1; also see Raha et al., 2023). MCDM methodologies can rank sub-watersheds (S-WSs) as per the intensity of active tectonics (Pourghasemi et al., 2021; Kumar and Sarkar, 2022). Analytical tools designed for this purpose prioritize the acquisition and evaluation of options within a set, incorporating relevant criteria into the assessment process.

Slope stability studies involve characteristics and structures of rock, the amount of water present, external loads acting on the slope and seismic activity. The Rock Mass Rating (RMR) and the Slope Mass Rating (SMR) are the two significant schemes to study slope stability. The RMR system evaluates the quality of a rock mass by considering factors such as strength and discontinuities characteristics. On the other hand, SMR is a modified version of RMR that considers the orientation of discontinuities relative to the slope face, providing a more customized evaluation of slope stability. These systems assist to forecast the future slope breakdowns and devising efficient stabilization methods (Kumar et al., 2017).

Paleostress inversion techniques widely used to derive the stress orientation by utilizing the fault plane data with slickenlines, recording the sense of movement (Hancock, 1985; Angelier, 1994; Vanik et al., 2018; Dasgupta et al., 2023). One of the ways to perform paleostress analysis is to presume that *(i)* the fault slips along the maximum resolved shear stress direction and *(ii)* the Wallace-Bott hypothesis is valid (Bott, 1959). The hypothesis assumes- *(i)* homogenous stress field, *(ii)* homogeneous lithology, *(iii)* no influence of local/small slip, *(iv)* fractures do not modify the existing stress field, and *(v)* weak planes do not rotate.

This work aims at deciphering the active tectonics of a part of Garhwal Himalaya, in the Bhagirathi river valley in terms of *(i)* morphometric study with TOPSIS and *(ii)* landslide studies involving kinematic analysis of the slopes, SMR and shearing properties of the slided material. We also perform *(iii)* paleostress analysis using Win-Tensor software (Ver 5.8.8) based on different kinds of meso-scale brittle fault data set and attempt to link past deformation with the present-day tectonics. We undertake the morphometric analysis from the TH, HH and LH of Bhagirathi river valley (Fig. 1). The aim is to study the geomorphic characters of a significant stretch of a single river. For fieldwork, landslide studies and paleostress analysis, we narrowed down to LH mostly along the same river section. The rationale of choosing a smaller area for field studies is that the entire stretch of the study area along the Bhagirathi river is too long (~ 260 km), whereas the studied stretch in the LH (~ 100 km) is reasonable to cover in the field.

2. Study area

2.1. Geology & tectonics

Cambrian to Silurian and Jurassic-Cretaceous sequences of the TH in the Garhwal section are (partly) deeper-water sedimentary deposits (Bhargava and Singh, 2020). The Neoproterozoic HHC possibly had a mixed source from southern Gondwana terranes and northern portion of south China (Imayama et al., 2023). Fore and back shears have been

Table 1
MCDM and TOPSIS applications in morphometric studies.

Authors	Terrain	Method(s)	Key conclusion(s)
Sadhasivam et al. (2020)	Dnyanganga basin, Maharashtra (India)	TOPSIS and Analytical Hierarchy Process (AHP) are used for soil erosion susceptibility mapping. Geometric variables and morphometric attributes computed using ArcGIS 10.2.	Highly susceptible sub-basin DNY16. Decision makers benefit from results for soil and water conservation planning.
Barman et al. (2021)	Chite Lui River (Mizoram, India)	TOPSIS was used for groundwater and soil erosion potential zone.	WS-A and WS-I are the highest and lowest susceptible to soil erosion respectively. WS-A and WS-I are also high and low groundwater potential zone respectively.
Biswas et al. (2021)	Lish and Jayanti River, North-Bengal, Kankuram and Kharswati river, Singbhum Craton, Jharkhand, Janauri-Chandigarh anticline (India)	Field survey with total station, Global Positioning System (GPS), clinometer for data collection. Statistical techniques viz., AHP and TOPSIS for data analysis. Use of high-resolution DEMs for tectonic indices application.	Tectonic impact on river channels and landscape topography analyzed. Field survey reveals changes in hydrological parameters and riverbed topography.
Al-Attar et al. (2022)	Greater Zab River Basin, Turkey-Iraq region	AHP and TOPSIS used for tectonic assessment.	The central part shows high tectonic activity due to fault interaction. Strike-slip faults influence drainage system patterns and sub-basin shapes.
Bahroudi et al. (2023)	Basiran-Mokhtaran area, eastern Iran	Multi-index overlay (MIO) and TOPSIS methods used for gold prospectivity mapping. Production-area (P-A) method for assigning weights to criteria in prospectivity mapping.	M-TOPSIS method slightly outperformed A, C, and M-TOPSIS versions. MIO detected 75 gold indications over 25% of the area. RS and lineaments layers ranked second, identifying 65 gold targets.
Kumar et al. (2022)	Mandakini basin Uttarakhand, India	WS prioritization and erosion-prone areas are demarcated with TOPSIS model.	The sediment production rate (SPR) model reveals that a significant portion (43.47%) of the basin is experiencing substantial erosion.
Malakar and Rai (2022)	Himalaya (covered complete Himalayan system)	Machine learning techniques were employed to identify spatial clusters of earthquakes in the Himalayan region. AHP and TOPSIS were utilized to estimate earthquake vulnerability.	Machine learning techniques identified 8 active earthquake clusters in the Himalayan region. Vulnerability assessment using MCDM models showed over 50% of the population faces high

(*continued on next page*)

Table 1 (*continued*)

Authors	Terrain	Method(s)	Key conclusion(s)
			earthquake vulnerability
Patel et al. (2022)	Ami River basin, Uttar Pradesh, India	AHP and TOPSIS used to rank the WS based on the soil erosion capability.	WSs XV and XVIII are highest and lowest susceptible to soil erosion, respectively.
Raha and Biswas (2022)	Jaldhaka basin (Sikkim and West Bengal, India)	Statistical methods like TOPSIS and VIseKriterijumska Optimizacija I Kompromisno Resenje (VIKOR) ranked tectonic activity of fans. X-ray diffraction (XRD) analysis is used to determine mineral composition and sediment compaction. Primary data collection included hydrological data and fan sediment sampling.	Meso-level fans ranked by tectonic activeness using statistical methods. Fan 2 is most tectonically active; Fan 4 is stable. Alluvial fan dynamics influenced by hydro-sediment interaction and tectonic instability.
Biswas et al. (2023)	Aizawl district Mizoram, India	Spring water suitable and spring water vulnerable sites demarcate based on the AHP-TOPSIS and VIKOR models.	WS map is prepared using TOPSIS and VIKOR model.
Patel et al. (2023)	Tapi river basin (Madhya Pradesh, Maharashtra), Surat (Gujarat), India	AHP, TOPSIS, VIKOR, Simple additive weighting (SAW) and Collaborative Filtering (CF) used for prioritizing erosion-prone areas. VIKOR method ranks alternatives based on conflicting parameters. Change indices and statistical tests used to assess model outcomes.	Morphometric analysis aids in prioritizing erosion-prone sub-WSs effectively. MCDA techniques classify sub-WSs into four priority classes based on scores. Implementation of soil conservation measures is vital for sustainable WS management.
Raha et al. (2023)	Madeira watershed, South America	TOPSIS is used to detect the influence of tectonic activity on the main and S-WSs. Analyzed the most and least active channels using TOPSIS for a comparative study.	WS 2 in Andean foreland area experiences higher tectonic activity and WSs in the Amazon cratonic area have lower levels of activity.
Roy et al. (2023)	Mayurakshi drainage system (Jharkhand & West Bengal, India)	Performed AHP with Principal component analysis (PCA) for erosion susceptibility assessment. Six principal components extracted with cumulative explained variance of 100%.	Erosion susceptibility is mainly low, except the middle Mayurakshi basin and Dwarka River. PCA integrated into AHP technique to assess erosion susceptibility.
Dzwairo et al. (2024)	Rietspruit catchment in Vaal basin, South Africa	Morphometric analysis using Shuttle Radar Topography Mission (SRTM) DEM and prioritization by AHP and TOPSIS.	Lithologically and structurally controlled terrain having low drainage intensity and density values. SW5 has the highest soil erosion susceptibility. Highest-ranked sub-basin has the lowest priority for soil erosion.
Puniya et al. (this study-2024)	Bhagirathi river valley, Uttarakhand (India)	AHP and TOPSIS used to assess the tectonically active sub-basins	Intensity of present-day tectonic activities in the 21 S-WS and the main Bhagirathi basin worked out.

reported from the HHC along the Bhagirathi river section (Mukherjee, 2013). Table 2 presents the most comprehensive lithologic succession in the entire LH in the Garhwal sector. The inner Lesser Himalaya (ILH) consists of paleo to Mesoproterozoic low-grade metamorphosed rocks, mostly quartzites, slates, limestones and schists. Metamorphic facies change drastically from greenschist (Berinag quartzites of ILH) to amphibolite [granite gneisses and mica schists of the MCT Zone] near the village Sainj towards north. Table 3 presents a review on morphometric and slope stability analyses from the Bhagirathi and the nearby basins.

The major thrusts in the field study area are MBT, TT, Berinag Thrust and MCT. Aglar and Basul Thrusts are the basal thrusts of the Deosari Syncline (Jain, 1971). TT is a stratigraphic contact between the Chandpur and the Rautgara Formation. Likewise, the Berinag Thrust separates the Berinag Formation thrust sheet from the Rautgara, Deoban and Mandhali Formation. The Berinag Thrust has been variously recognized locally as Uttarkashi Thrust (UT), Dunda Thrust (DT), Singuni Thrust (ST) and Dharasu Thrust (DhT) (review in Bose and Mukherjee, 2019). As per the K–Ar (muscovite) and Ar/Ar (hornblende) dates, MCT in the Garhwal Himalaya activated during 19.8 ± 2.6 and 5.9 ± 0.2 Ma (Metcalfe, 1993; Catlos et al., 2002). The MBT slipped in the western Himalaya during the Miocene (Meigs et al., 1995). Folding happened at least twice in the Garhwal Lesser Himalaya (Agarwal & Kumar, 1973).

Biswas et al. (2022) based on paleostress studies deciphered orogen-parallel shears along 130°–310°N, probably during ~ 15-5 Ma, from this study area. Obscure pre-Himalayan deformation and various local structural detail has been compiled from the Garhwal Himalaya (repositories 1 and 4, respectively, in Biswas et al., 2022). Several landslides in the past have been also compiled from the Bhagirathi river section by Biswas et al. (2022, their Fig. 5 and repositories 6, 7).

2.2. Rivers

The Bhagirathi River, originating from Gangotri glacier of Garhwal Himalaya region, is the primary tributary of the Ganges river system. Alaknanda River, which originates from the Bhagirath Kharak and Satopanth Glaciers joins Bhagirathi at Devprayag. Together, they form the mountainous catchment of the Ganges. Bhagirathi River exhibits both erosion and depositional terraces with Quaternary sediments (Das and Sangode, 2022) spanning from Harshil to Gangnani (in the HHC). Such terraces are also particularly prominent in the Uttarkashi and at Dunda (within the LH).

3. Theory & methodology

3.1. Morphometry

3.1.1. Morpho-tectonic parameters

The hydrological boundaries of the Bhagirathi River main WS along with its 21 sub-basins/sub-watersheds (S-WSs) were delineated and analyzed morphologically (Fig. 2). Morphometric parameters were derived from the river network delineated using the Shuttle Radar Topography Mission (SRTM), Digital Elevation Model (DEM) with 30 m

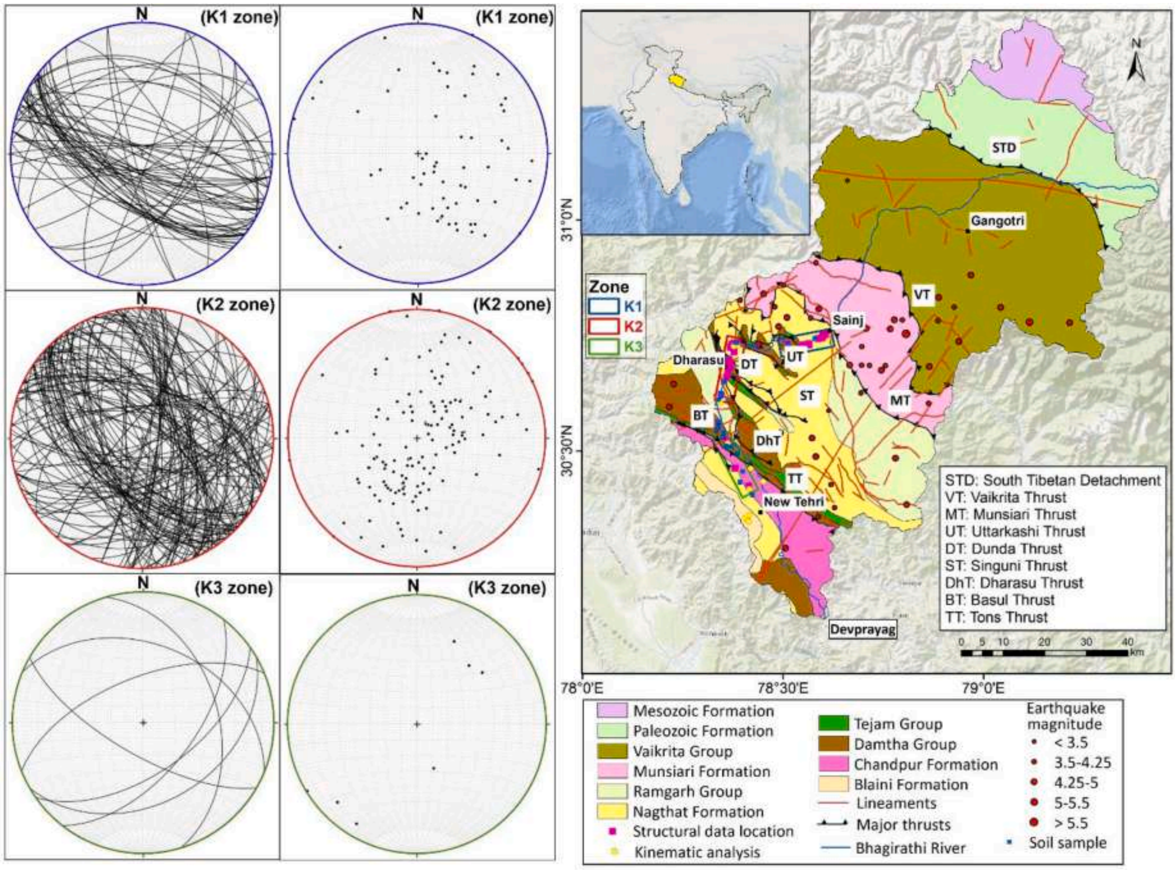

Fig. 1. Geologic map of the Bhagirathi river basin. Lithology and seismic data reproduced from Internet ref (1,2). Great circles in the stereoplot: fault plane. Black dots in stereoplot: lineations developed on the fault planes.

spatial resolution (Internet reference 3). The delineation of S-WSs exclusively relied on third and higher order streams (Strahler, 1952). Areal, relief and linear features were assessed using the ArcGIS software (ver. 10.8).

TOPSIS is a quantitative decision-making tool rooted in distance-based analysis. It calculates the Euclidean distance from a given alternative to both positive and negative ideal solution (Hwang and Yoon, 1981; Kumar and Sarkar, 2022). It facilitates ranking of regional entities as per their attributes by identifying the alternatives, which are nearest to the Positive Ideal Solution (PIS) and farthest from the Negative Ideal Solution (NIS) (Chen, 2000). Tectonic prioritization of S-WSs of Bhagirathi river basin through the application of morphometric indices has been evaluated at both linear and basin scales. TOPSIS was run based on the following seven parameters: asymmetric factor (AF), basin shape (Bs), circularity ratio (R_c), form factor (F_f), hypsometric integral (HI), relief ration (R_h) and transverse topographic symmetry (T) (Table 4).

3.1.2. Basin prioritization using TOPSIS model

The aforementioned indices were applied to analyse the 21 sub-basins within the study area to evaluate their recent tectonic activity. Morphometric indices were computed to determine ideal and anti-ideal points, where $L_{ur} = 0.1–53341.6$ and $D_D = 0.30–0.52$ indicate higher tectonic activity. On other hand, higher SI and lower AF connote lower tectonic activity. S-WSs were classified based on these calculated values. The selection of the most suitable morphometric indicator was determined by its proximity to the PIS and its distance from the NIS. The analysis was performed using Microsoft Excel (Microsoft 365) for precise computation and assessment. Fig. 3 presents the salient steps and are as follows:

Step 1: Creation of a decision-matrix for ranking (using the calculated indices)

A1, A2 … There are several potential options. C1, C2 … Cn represent the standards used to evaluate the different performances. X_{ij} represents the ranking of an alternative in relation to criteria.
Step 2: Calculation of the normalized decision matrix.

$$n_{ij} = \frac{x_{ij}}{\sqrt{\sum_{i=1}^{x_{ij}} X_{ij}^2}} \tag{1}$$

Step 3: Calculation of the weighted normalized

$v_{ij} = w_j * n_{ij},\ i = 1, \ldots, m, j = 1, \ldots, n$
The weights were calculated using the AHP.

Step 4: Identification of the PIS (A+) and NIS (A-)

$$A+ = ((\max vij \mid j \in J), (\min vij \mid j \in J') \mid i = 1, 2, \ldots, m) = \{v_1^+, v_2^+ \cdots\cdots V_m^+\} \tag{2}$$

$$A- = ((\min vij \mid j \in J), (\max vij \mid j \in J') \mid i = 1, 2, \ldots, m) = \{v_1^-, v_2^- \cdots\cdots V_m^-\} \tag{3}$$

J and $J^{/}$ are linked with positive & negative conditions, respectively.
Step 5: Calculation of the partition methods by using the n-dimensional Euclidian distance. The separation from PIS is:

$$S_i^+ = \sqrt{\sum_{j=1}^{n} \left(V_i^+ - V_{ij}\right)^2}\ i = 1, 2, \ldots m \tag{4}$$

Table 2
Litho-tectonic succession of the LH (Garhwal region), as compiled by Biswas et al. (2022). Stratigraphic units on which field data were collected are in ***green***.

	Formation (Age)	Lithology & key-features
MAIN BOUNDARY THRUST		
OUTER LESSER HIMALAYA (OLH)	**Tal Formation** (Cambrian-Ordovician/ Jurrassic to Cretaceous/Lower Cambrian)	Rich argillaceous matter of greenish-grey shale, black phosphorite-chert, bluish grey limestone altered with white purple quartzite deposited under shallow marine to inter tidal condition
OUTER LESSER HIMALAYA (OLH)	**Krol Formation** (Cambrian/ Permian to Triassic/Early Cambrian/ Neoproterozoic)	Blue and black colored limestones altered with yellow-white, grey and buff colored quartzite and purple green, greyish green, black carbonaceous phyllite.
OUTER LESSER HIMALAYA (OLH)	**Blaini Formation (**Permo-(Carboniferous/ Neoproterozoic)	Greenish-grey boulder conglomerate layers with sedimentary and low-grade metamorphic provenance, along with carbonaceous as well as green-purple shale, grey siltstone, grey and purple dolomite, grey limestone, grey quartzites with non-fossiliferous glacio-marine origin.
OUTER LESSER HIMALAYA (OLH)	**Nagthat Formation** (Neoproterozoic)	Sericite schistose quartzites, purple, white and green quartz arenite, altered with shale and phyllites deposited under shallow tidal-sandbar zone
OUTER LESSER HIMALAYA (OLH)	**BASUL THRUST AND AGLAR THRUST**	
OUTER LESSER HIMALAYA (OLH)	**Chadpur Formation/ Dharmandal Group/ Saryu Formation/ Dharasu Formation (Neoproterozoic)**	Greyish green phyllite intercalated with grey and very fine metasiltstone and buff, grey metagraywacke, pinkish brown sublitharenitic quartzite occurring in massive habit.
TONS THRUST (SRINAGAR, NORTH ALMORA, DHARKOT, CHAIL-3 THRUST)		
INNER LH HIMALAYA (ILH)	**Rautgara Formation/ Kotga Banali Group/ Dunda Slate** (Neo-Mesoproterozoic)	Muddy quartzite (subgreywacke to sublitharenite) altered with grey-greenish and purple color phyllite and green, purple, greyish black color slate. Ripple marks and mudcracks indicate delta deposit.
INNER LH HIMALAYA (ILH)	**Deoban Formation** (Neoproterozoic)	Thick layers of stromatolite-cherty dolomites altered with quartzite and grey slates deposited under shallow marine condition.
INNER LH HIMALAYA (ILH)	**Mandhali Formation** (Neoproterozoic / Paleoproterozoic)	Blue and black colored limestones altered with yellow-white, grey and buff colored quartzite and purple, green, greyish green, black carbonaceous phyllite.
	BERINAG THRUST (UTTARKASHI, DUNDA, SINGUNI, DHARASU THRUST)	
	Berinag Formation/Gamri Quartzite Dichli dolomite/ Pratapnagar Group/ Garhwal Group (Mesoproterozoic/ Paleoproterozoic)	Thick bedded of sugary sericitic quartzite, pinkish white to light green quartz arenite with little chlorite schist alteration. Oldest formation of LHS.
MUNSIARI THRUST		
MCT ZONE SCHISTS		

Table 3
Morphotectonic and slope stability studies in Bhagirathi and nearby river valleys.

Author	Terrain	Key conclusion(s)
Gupta and Anbalagan (1997)	Tehri dam reservoir, Uttarakhand (India)	Most of the area in the reservoir is under low-moderate hazard category.
Saha et al. (2002)	Between Lohari-Nag to Uttarkashi, Bhagirathi river valley, Uttarakhand (India)	Distribution of the landslides majorly governed by the close proximity (<500 m) to the thrust/fault zones.
Bali et al.(2003)	Gangotri glacier valley, Uttarakhand (India)	Neotectonic influences shaped the geomorphic evolution of the region. U-shaped valleys significantly exposed to fluvio-glacial denudational processes developed V-shaped valleys.
Gupta et al. (2006)	A part of Bhagirathi river valley, Uttarakhand (India)	5.4% of the area is under very high hazard zone, 30.7% in high, 52.5% in medium and 11.7% area in low to very low hazard area.
Chakraborty and Anbalagan (2008)	Uttarkashi-Bhatwari road section, Uttarakhand (India)	Slopes are generally stable but in monsoon season, these can be unstable due the saturation. Slopes having > 50 angle may be stable. To avoid the instability of the slope, 1–1.5 m toe wall should be provided.
Srivastava et al. (2009)	Tons river (Uttarakhand and Himachal Pradesh, India)	Information value method used for landslide hazard zonation. Around 78.6% of active landslides are concentrated in areas classified as Very High (55.4%) and High (23.2%) hazard zones.
Selvan et al. (2011)	Bhagirathi river valley, Uttarakhand (India)	High drainage density shows much uneven surface in glacier region. Slopes are structurally controlled
Shukla et al. (2014)	Alaknanda river valley, Uttarakhand (India)	Earthquake density (unitless) peaks in very high seismic zones (0.052), followed by high (0.035), moderate (0.016), and low zones (0.011). The frequencies of landslides in the very high zone measures a density of 0.013, indicating 20 landslides, while in the moderate zone exhibits a density of 0.010 with 35 landslides. Intense tectonic activity is concentrated along the boundary of MT and Ramgarh Thrust (RT) within the study area.
Ballabh et al. (2014)	A part of Bhagirathi river valley, Uttarakhand (India)	The main cause of the landslides is road development project. Freeze-thaw and removal of slope toes in road cutting are also main causes for the disturbance in slope.
Bhattacharjee (2015)	Bhagirathi river, Uttarkashi district, Uttarakhand (India)	Drainage density and relief are high near Bhatwari, Gangnani and Bhairo-Ghati areas.
GSI (2016)	Bhagirathi river, Uttarkashi district, Uttarakhand (India)	Maps showing landslides prepared. Most of the slides in Saknidhar, Chandpur and Nagthat Formation
Gupta et al. (2016)	Between Uttarkashi and Bhatwari, Uttarakhand (India)	River gradient between Bhatwari and Uttarkashi ranges 3.66–66.6 m km^{-1}. River is steepest within the MCT zone. Several landslides happened within the MCT zone. Zones between Bhatwari to Ganeshpur and Ganeshpur to Uttarkashi are characterized by transportation and deposition of sediments, respectively. Most of the landslides in the area occurs where hill slope angle exceeds 45^0 and the friction angle ranges $26.1–33.33^0$. The cohesion value ranges 0.06–0.17 kg m^{-2}.
Kamal et al. (2016)	Bhagirathi & Alaknanda Basins, Uttarakhand (India)	Mean bifurcation ratio shows that Bhagirathi basin is more structurally disturbed than the Alaknanda Basin.
Mehta et al. (2018)	Bhagirathi river valley, Uttarakhand (India)	There are two zones, which can be vulnerable in extreme events: Zone I, situated beyond the MCT, exhibits intense tectonic deformation and thrusting of rocks, resulting in steep hill slopes. This region receives highest precipitation. Conversely, Zone II, positioned in lower elevations, features gentler hill slopes and less intense rainfall. However, due to higher population density, anthropogenic activities, and the presence of weak rocks like phyllites, certain areas in this zone experienced failure. Concentration of damaged roads and a high incidence of landslides in the LH identified.
Tewari et al. (2019)	Gangotri town to Gangotri glacier, Uttarakhand (India)	Denudation at the right bank is higher than that at the left bank. This area is highly vulnerable to the flood during monsoon.
Ahmad and Khan (2020)	Bhagirathi valley, Uttarakhand (India)	High Hypsometric Integral (HI) observed in certain glaciated WSs connotes tectonic disturbance resulting from ongoing glacier erosion occurring at high altitudes near the snowline.
Taloor et al. (2021)	Mandakini & Bhilangana basin, Uttarakhand (India)	Morphology of Bhilangana and Mandakini changing significantly primarily due to tectonic activities.
Das and Sangode (2022)	Alaknanda & Bhagirathi valley, Uttarakhand (India)	High rate of erosion (2.87 mm y^{-1}) within the MCT zone. The main factor of the erosion may be the fluvial process. Differential tectonic uplift predominantly governs topographic evolution, with rainfall acting as a secondary factor.
Chauhan and Dixit (2023)	All districts of Uttarakhand (India)	Uttarkashi, Chamoli, Rudraprayag, Bageshwar and Pithoragarh districts exhibit pronounced relief parameters due to intense tectonic activity. Drainage networks in Uttarkashi, Chamoli, Pithoragarh and Nainital reflect active tectonics.
Patidar et al. (2024)	Mandakini River Basin, Uttarakhand (India)	The Stream Power Incision Model (SPIM) analysis of the Mandakini River basin reveals uplift in the upper basin. Here, AF ~32 and T = 0.25–0.37 indicate leftward migration of the mainstream. The lower basin displays AF = 70 and

(*continued on next page*)

Table 3 (*continued*)

Author	Terrain	Key conclusion(s)
		T = 0.38–0.42 suggesting a rightward migration of the mainstream, accompanied by accelerated vertical uplift and incision.
Puniya et al. (2024-this study)	Bhagirathi river valley, Uttarakhand (India)	AF is high and low for WS 17 and WS 16, respectively. Wedge and planar failure occurred near DhT, DT and TT. Soil from slided materials have low cohesion.

The separation from the NIS is;

$$S_i^- = \sqrt{\sum_{j=1}^{n} \left(V_i^- - V_{ij}\right)^2}\ \mathrm{i} = 1, 2, \ldots \mathrm{m} \tag{5}$$

Step 6: Calculation of the relative closeness to the ideal solution.

$$C_i^+ = \frac{S_i^+}{S_i^+ + S_i^-} \tag{6}$$

3.2. Slope stability analysis

This was carried out for 11 selected slopes (Fig. 4). We undertook RMR, kinematic slope analysis and SMR. We tested uniaxial compressive strength (UCS) using the Schmidt hammer method, adhering to the recommended guidelines by the International Society for Rock Mechanics (ISRM) (Bieniawski, 1989; ISRM, 2007). We documented spacing, aperture, roughness, type of filling and weathering conditions of joints. Additionally, kinematic analysis of the slope has been conducted using stereographic projection techniques using the Stereonet software (ver. 11.6.0, year 2023). This facilitates comprehensive analysis of potential failure modes within rock masses. Kinematics, in this context, refers to the analysis of motion of objects without consideration of the natural forces influencing their movement (Goodman, 1989).

SMR can be derived from RMR by incorporating adjustment factors (Romana 1985):

$$SMR = RMR + F_1F_2F_3 + F_4 \tag{7}$$

Here

$$F_1 = (1 - \mathrm{Sin}\ A_1)^2 \tag{8}$$

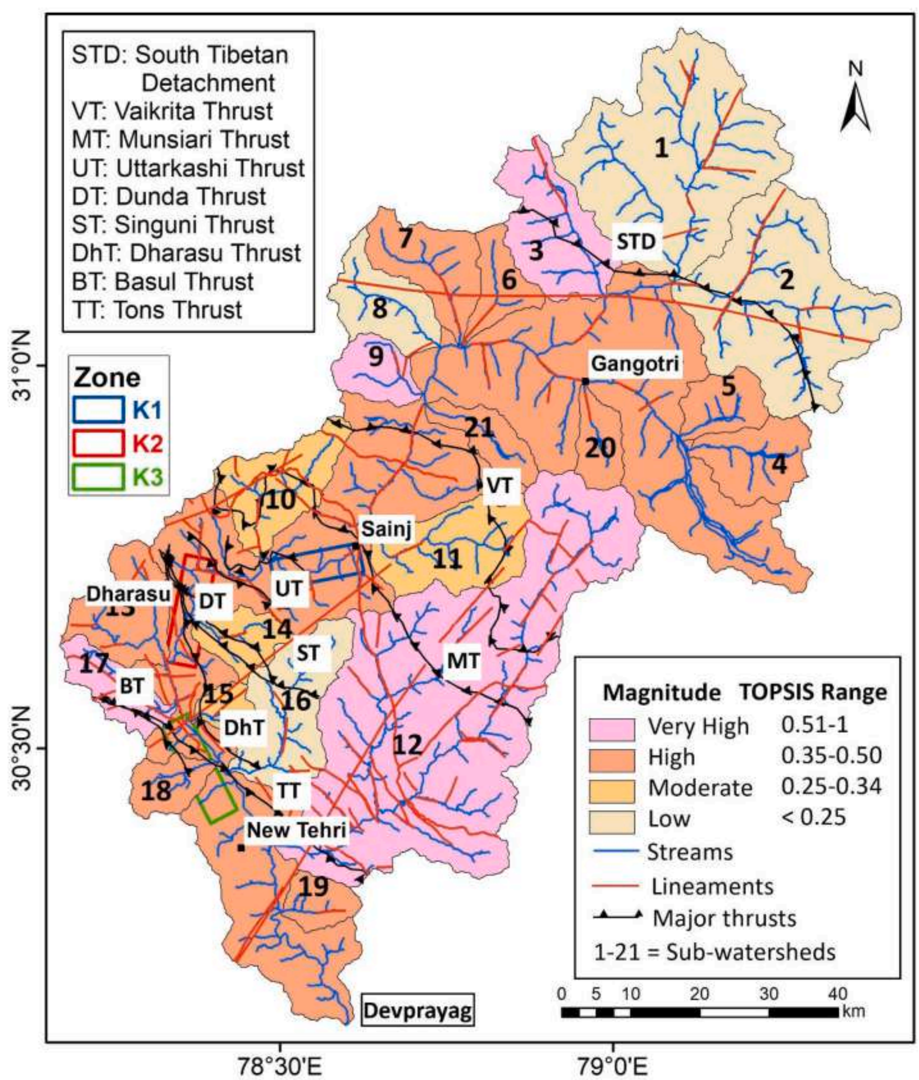

Fig. 2. Tectonically active WS map based on TOPSIS analysis.

Table 4
Parameters and formulas used in current study for morphotectonic/TOPSIS analysis.

Parameters	Formula	Reference
Drainage density (D_D)	$D_D = L_u/A$ L_u = Cumulative stream length A = Area	Horton (1932)
Form factor (F_f)	$F_f = A/L_b^2$ A = Area L_b = Stream length	Horton (1932)
Drainage texture (D_t)	$D_t = N_u/P$ Nu = Stream number P = Perimeter	Horton (1945)
Stream number (N_u)	$N_u = N_1 + N_2 + \ldots N_n$ N_1, N_2= Stream number	Horton (1945)
Stream order (S_u)	Hierarchical Rank	Strahler (1952)
1st order stream (S_{uf})	–	Strahler (1952)
Hypsometric Integral (HI)	$HI = (H_{mean} - H_{min})/(H_{max}–H_{min})$ H = Elevation of the catchment $H_{mean,}$ H_{max} and H_{min} are the mean, maximum and minimum values of H, respectively	Strahler (1952)
Circulatory ratio (R_c)	$R_c = 4\pi AP^{-2}$ A = Area of the watershed P = Perimeter of the watershed	Miller (1953)
Elongation ratio (R_e)	$R_e = 2{*}L_b^{-1}(A/\pi)^{0.5}$ A = Area of the watershed L_b = Stream length	Schumm (1956)
Relief ratio (R_h)	$R_h = H/L_b$ H = Total relief of basin L_b = Stream length	Schumm (1956)
Stream length (L_u)	$L_u = L_1 + L_2 + \ldots L_n$ L_1, L_2 = Lengths of each stream segment	Strahler (1964)
Stream length ratio (L_{ur})	$L_{ur} = L_{u.}(L_{u\text{-}1})^{-1}$ L_u = Stream length $L_{u\text{-}1}$ = Mean length of the stream segments of the next lower order	Strahler (1964)
Sinuosity (in highest order) (SI)	SI = Length of stream channel of highest order/Straight line distance of same stream	Mueller (1968)
Basin Shape (B_s)	$B_s = Bl\ B_w^{-1}$ Bl = Measured length from headwater to the point on the mouth of the basin B_w = Measured width at the widest point on the basin	Bull and McFadden (1977); Ramírez-Herrera (1998)
Asymmetric factor (AF)	$AF = (A_r A_t^{-1}){*}100$ A_r = Area of basin to the right of the stream A_t = total area of basin	Hare and Gardner (1985)
Transverse topographic symmetry (T)	$T = D_a\ D_d^{-1}$ D_d = Distance from the basin's midline to the basin divide. D_a = Distance from the drainage basin's midline to the meander belt's midline	Cox (1994)

A_1: angle between joint strikes and slope orientation. F_1 is calculated by angle between joint strikes and slope face. F_1 ranges 1–0.15.

$$F2 = \tan^2 B_j, \tag{9}$$

B_j: joints' dip in planar failure. It ranges 1–0.15. F3: correlation factor between joint dip angles and slope face. F4: excavation method adjustment factor.

Grain size analysis of the landslide soil was undertaken to categorize soil types. Grain size analysis test is carried out based on the IS 2720–4 (1985) (Internet reference 4). Direct Shear Test (DST) is conducted based on the IS 2720–13 (1986) (Internet reference 5). In DST, soil specimens are sheared under consistent normal stresses of 50, 100, and

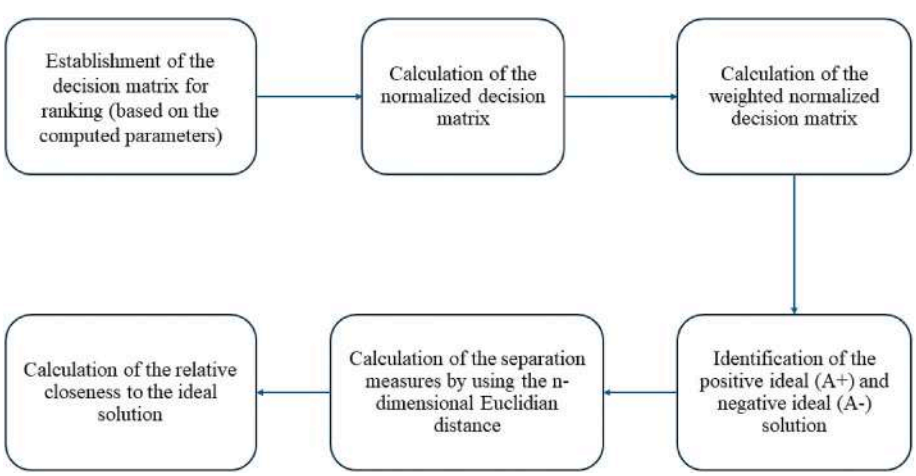

Fig. 3. Steps followed for the TOPSIS analysis as per Aouragh and Essahlaoui (2018).

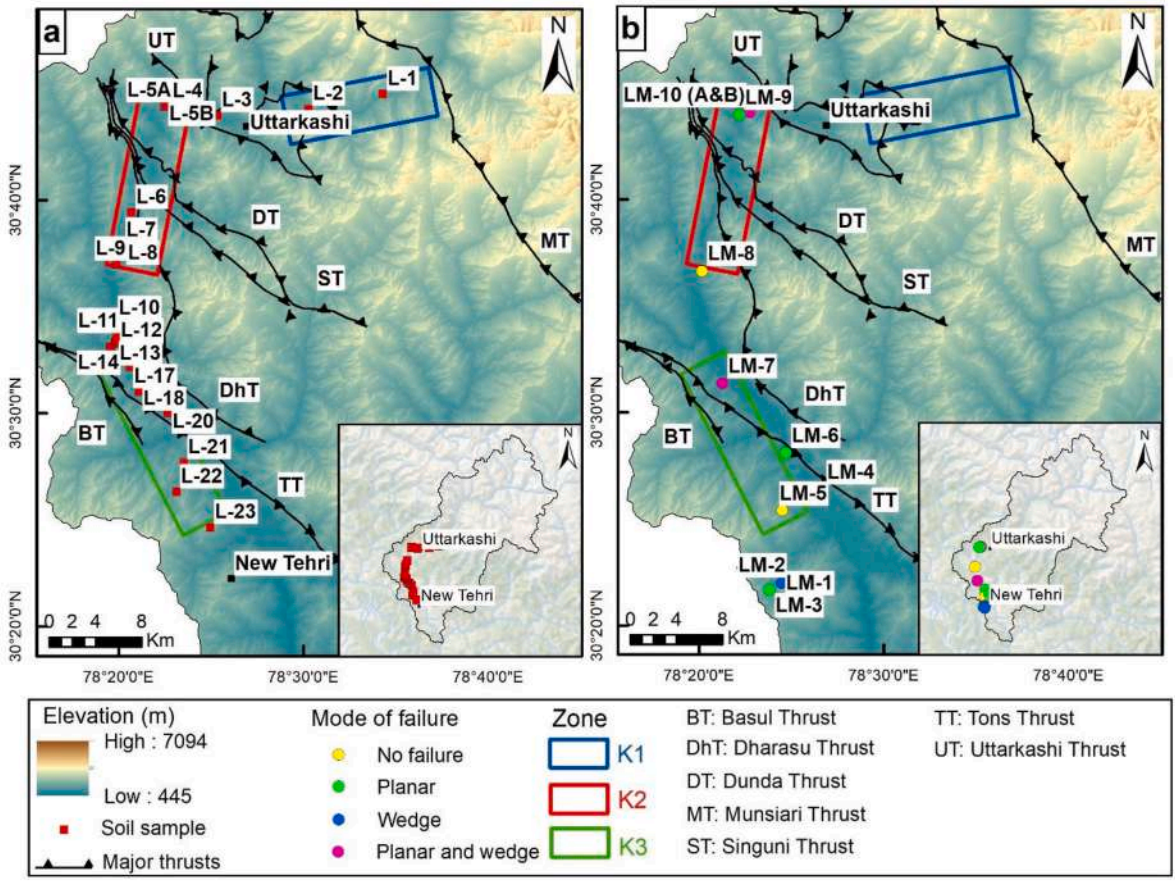

Fig. 4. K1, K2 and K3 zones showing locations for **(a)** soil sampling and **(b)** kinematic analysis.

150 kN m^{-2} at three different instants. Natural moisture content is calculated dry oven method based on IS 2720–2 (1973) (Internet reference 6, 1973). Total 24 samples have been collected and tested from different slides (Fig. 4).

3.3. *Structural geology & paleostress analysis*

Brittle faults have been studied only from the ILH. Fault planes can provide insights into the stress regime and tectonic processes at play. We collected 254 data on fault-planes and slickenlines from three zones (K1, K2 and K3) along the Rishikesh-Gangotri highway in the Garhwal LH (Table 5; Figs. 1 and 4). The observed faults are exposed for about half a meter length or less in most cases, and no cross-cut relationship was observed. The relative time relation amongst the different kinds of faulting (reverse, normal and strike-slip) therefore remains indeterminate. Also, being documented first time through this study, absolute timings of strike-slip and normal faulting from these zones are unavailable. Based on morphology, Doblas (1998) grouped 61 different types of slickensides kinematic indicators associated with brittle shear zones/-faults into 11 main categories. The classification also explained how shear sense was inferred from the scale of occurrence of features, which ranged from microscopic to hand specimen to outcrop. In the field, we used Doblas (1998) to determine the specific type of slickensides and utilized their orientations for the analysis of paleostress. Particularly we have found ST-2, ST-3 and ST-5 types of slickensides of Doblas (1998). Repository R1 presents theoretical detail on lineations developed on fault planes.

K1 zone: From this zone, 76 data of fault planes and slickenlines were recorded. Forty-one fault planes dip towards S to SW (e.g., Fig. 5a–d) (Repository R2). Prominent lineation of ST3 type of Doblas (1998) was documented on near-planar fault planes from the Nagthat Formation and the Damtha Group. The other kinds of lineations that were documented are ST2 and ST5 (Repository R2).

K2 zone: From this zone, 171 data of fault planes and slickenlines were recorded. Thirty-three fault planes dip towards N to NE (e.g., Fig. 6a–d) and thirty-two fault planes dip towards NE to E (Repository R2). ST3 type of Doblas (1998) are the prominent types of lineations documented on (sub)planar fault planes from the Damtha Group, Tejam Group and from the Nagthat Formation. The other kinds of lineations that were documented are ST2 and ST5 (Repository R2).

K3 zone: Only seven fault planes are recorded in this zone. These fault planes dip in different directions (N, E, SE, S, SW and NW). In one case the fault plane has no visible lineations (Fig. 7a), in few cases lineations are doubtful (Fig. 7b and c), and seldom they are moderately well developed (e.g., Fig. 7d).

The field-recorded data on attitudes of faults and slickenlines are run through the WinTensor (ver. 5.8.8) program (Delvaux, 1993; Delvaux et al., 1997; Delvaux and Sperner, 2003) to perform the paleostress analysis. Apart from generating orientation of the stress field by the Right Dihedron Method, this software has an edge over other paleostress software in deriving stress regimes in terms of stress index ($R^{/}$) (Delvaux et al., 1997; Delvaux and Sperner, 2003). The stress regime works as a function of the stress ratio (detail in Delvaux et al., 1997; Delvaux and Sperner, 2003). The results display the paleostress regime(s) in terms of the principal stress tensors ($\sigma_1 \geq \sigma_2 \geq \sigma_3$).

Our fieldwork from NW Lesser Himalaya recorded three types of fault movements- *(i)* normal slip, *(ii)* reverse slip, and *(iii)* strike slip. The stress fields were obtained by dividing the dataset based on these

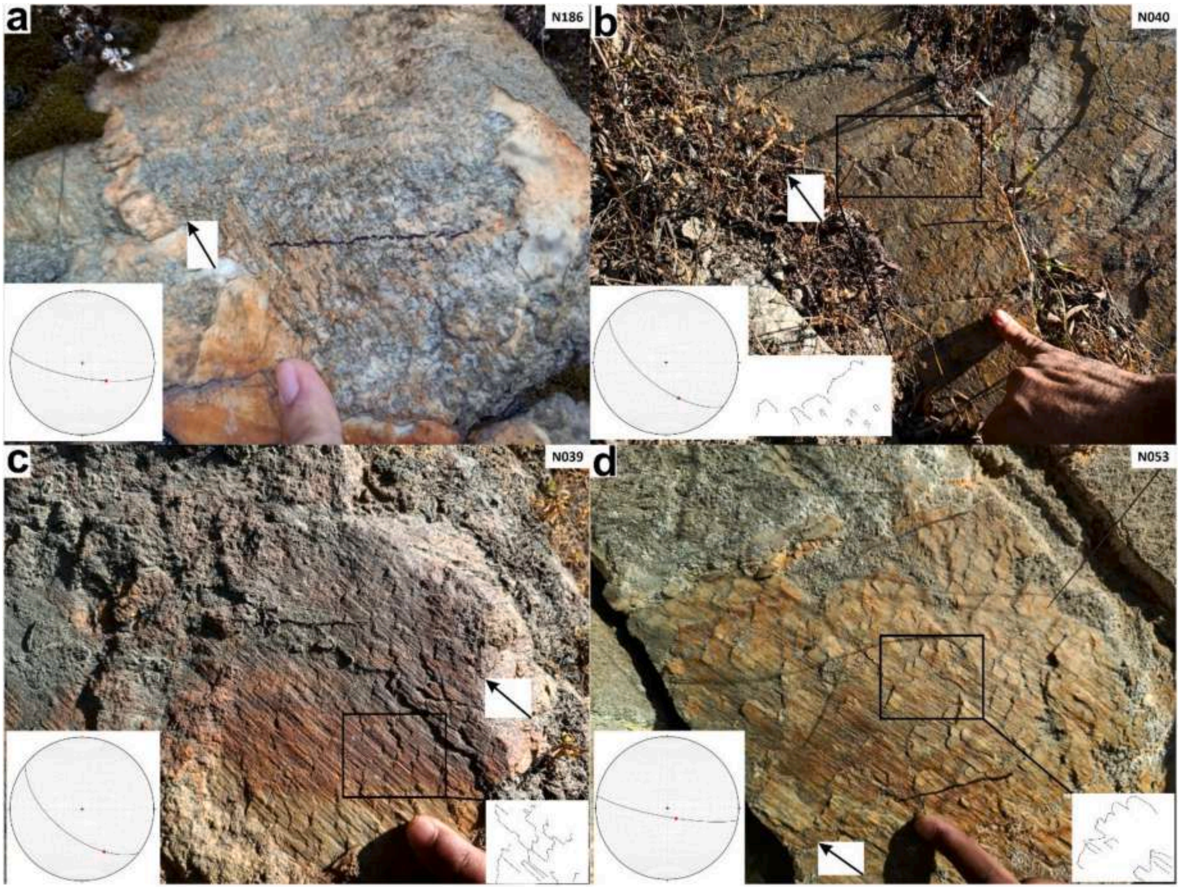

Fig. 5. Examples from K1 zone. Finger nail marker ~ 1.5 cm. Great circles in the stereoplot: fault plane. Red dot on the great circles: lineations developed on the fault planes. Arrow: slip direction of the missing block. **a.** Prominent lineation- ST3 (as per Doblas, 1998) and slickolite planes (as per Twiss and Moores, 2006), quartzite, Nagthat Formation. **b.** Prominent lineation- ST3 (as per Doblas, 1998) and slickolite planes (as per Twiss and Moores, 2006) (similar to Fig. 3.30 of Mukherjee, 2015b), quartzite, Nagthat Formation. **c.** Prominent lineation- ST3 (as per Doblas, 1998) and slickolite planes (as per Twiss and Moores, 2006), (similar to Fig. 3.29 of Mukherjee, 2015b), schistose quartzite, Nagthat Formation. **d.** Prominent lineation- ST3 (as per Doblas, 1998) and slickolite planes (as per Twiss and Moores, 2006), (similar to Fig. 3.28 of Mukherjee, 2015b), quartzite, Nagthat Formation.

Table 5
Zone-wise distribution of fault-planes and slickenlines data collection points. Zones K1, K2 and K3 are shown in Fig. 4 n: Total number of data.

Direction	K1 (n = 76)	K2 (n = 171)	K3 (n = 7)
N-NE	13	33	1
NE-E	3	32	1
E-SE	5	22	1
SE-S	3	20	2
S-SW	41	31	1
SW-W	5	24	0
W-NW	0	3	0
NW-N	6	6	1

slip senses. The paleostress results were obtained after applying the Right Dihedron method to the above-mentioned fault planes (Figs. 1 and 4). Within the WinTensor (ver. 5.8.8) software, for normal slip the rake is represented as a negative value, and it is positive for reverse slip. Based on the confidence level, fault plane movements are further categorized into *(i)* C- certain, *(ii)* P- probable, *(iii)* S- suppose, and *(iv)* X- unknown. Unknown slip data are used for normal as well as reverse slip by assigning minimum weight to them.

4. Results

4.1. Morphometry

The S-WSs within the Bhagirathi River basin, and the entire main watershed itself exhibit varying degrees of asymmetry, as quantified by the AF values (2.41–28.01). The maximal value of AF, reaching 28.01, is observed for the S-WS-17 and the minimum (2.41) is for S-WS-16. S-WS-13 also shows a higher AF value (16.06). The sinuosity index quantifies channels' deviation from linear paths, reflecting the influence of structures/tectonics. Sinuosity value for the highest order (sixth order) stream in the main watershed is 1.7. S-WS-2, 19 and the main WS have the same and maximum elongation ratio (0.42). S-WS-12 has the minimum elongation ratio (0.22). Circularity ratio (R_c) is maximum (0.74) for S-WS-19. Very low R_c is calculated for the main WS (0.28) and the S-WS-12 (0.33). S-WS-17 has the highest Bs value (3.35), while S-WS-2 has the lowest Bs value (0.97). The main WS has the Bs = 2.86. The Transverse Topographic Symmetry Factor (T) serves as a quantitative indicator delineating the degree of departure of primary channels from the central axis of the associated WSs. This metric offers valuable insights into the spatial alignment of river networks and their topographic context. S-WS-2 has the minimum T value of 0. 01, and S-WS-9 has the highest T value of 0.82. The main WS has T = 0.43 (Table 6).

As per the TOPSIS model, S-WS-3, 9, 12 and 17 exhibit highest tectonic activity (under very high class; 0.51–1), whereas S-WS-1, 2, 8 and 16 the least (low; <0.25). The primary channel WS of the Bhagirathi

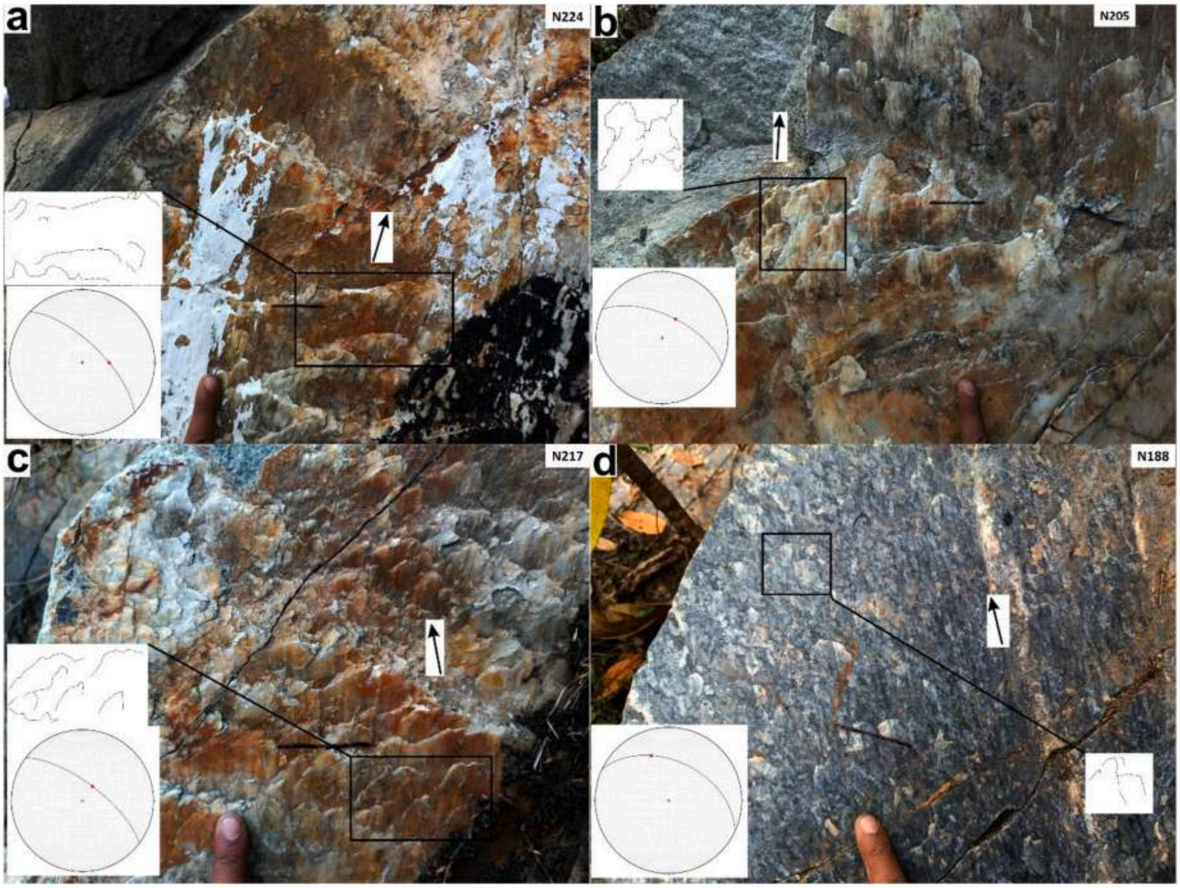

Fig. 6. Examples from K2 zone. Finger nail marker ~ 1.5 cm. Great circles in the stereoplot: fault plane. Red dot on the great circles: lineations developed on the fault planes. Arrow: slip direction of the missing block. **a.** Prominent lineation- ST3 (as per Doblas, 1998) and slickolite planes (as per Twiss and Moores, 2006), quartzite, Tejam Group. **b.** Prominent lineation- ST3 (as per Doblas, 1998) and slickolite planes (as per Twiss and Moores, 2006), (similar to Fig. 3.28 of Mukherjee, 2015b), quartzite, Tejam Group. c. Prominent lineation- ST3 (as per Doblas, 1998) and slickolite planes (as per Twiss and Moores, 2006), (similar to Fig. 3.30 of Mukherjee, 2015b), quartzite, Tejam Group. **d.** Moderately visible lineation, ST5 (as per Doblas, 1998) and slickolite planes (as per Twiss and Moores, 2006), quartzite, Tejam Group.

basin attains under class 2 (high) (Fig. 2). A comparative analysis was conducted to assess the tectonic activity within the most and least active S-WSs. This comparison is indicated by longitudinal profiles with SL. R2 study also has been done and Table 7 presents the S-WS ranks. It shows that out of 21 master streams of S-WSs, 11 streams have rank 1 showing high tectonic activity. Master stream-14 is least active. As shown in the slope map (Fig. 8), ~ 67% area of the entire Bhagirathi basin chosen in this study has slope of 15–45°. Around 14.5% area has very gentle slopes having 0–15° slope. ~ 9% area has slopes >45°. ~ 26.3% slope faces between south to west, ~ 25.2% north to east facing, ~ 24.4% east to south facing and ~ 24.1% slopes are west to north facing.

Sun-facing slopes with steep angles are more susceptible to instability. Due to the freeze-thaw process, these slopes are highly vulnerable to erosion and joint weakness, making them extremely unstable.

4.2. Landslide studies

Out of the studied 11 slopes, two are prone to wedge failure, four to planar failure, three to both planar & wedge failure, and only two are stable (Figs. 9 and 10). RMR values show that mostly the rocks are of Class-III category and can be prone to landslide. SMR values range from 7 to 50. SMR values are low for most of the slopes. All the slopes have <20 SMR except the locations 5, 6 and 8 (SMR = 42, 37 and 50, respectively). SMR values of <20 shows that slopes are vulnerable and are prone to failure (Table 8). Kinematic analysis of the slopes is shown in Repository R3.

The grain size analysis of the soil samples collected from 24 locations within the LH indicates that most of them are gravelly sand (Table 9). Cohesion values vary for each location (Table 9). Samples from locations 3 (Nagthat Formation), 9 (Ramgarh Group), 13 (Tejam Group) and 16 (Chandpur Formation) have very low cohesion or are cohesionless. For other samples, cohesion ranges between 0.13 and 0.83 kg cm^{-2}. Friction angle ranges between 2.41 and 35.26°. High moisture can locally reduce cohesion at few places. Moisture content ranges 3.4–11.9%. Slopes having less cohesion value or cohesionless strata can be very prone to slope instability. Lab testing results and graphs are presented in Table 9 and Repository R4.

4.3. Paleostress analysis

Paleostress analysis on 145 normal slip movements discloses a marginal radial extensive regime with the tensor characterized by σi = plunge/trend: σ1 = 83°/302°, σ2 = 06°/103°, and σ3 = 02°/193° with a stress regime index R$^{/}$ = 0.25 (Table 10). Extension took place along NNE-SSW (Fig. 11). From the studied NW Lesser Himalayan terrain, an abundance of reverse slip movement is characterized by σ1 = 01°/030°, σ2 = 05°/300°, and σ3 = 85°/135° with an NE-SW direction of maximum compression with a small radial component and the stress regime index of 2.69 (Fig. 11b). A pure strike-slip movement was also noted with σ1 = 10°/023°, σ2 = 77°/240°, and σ3 = 07°/115° calculated from 11 fault planes with a stress index of 1.48 (Fig. 11c). The dataset used to derive paleostress results is compiled in Repository R5.

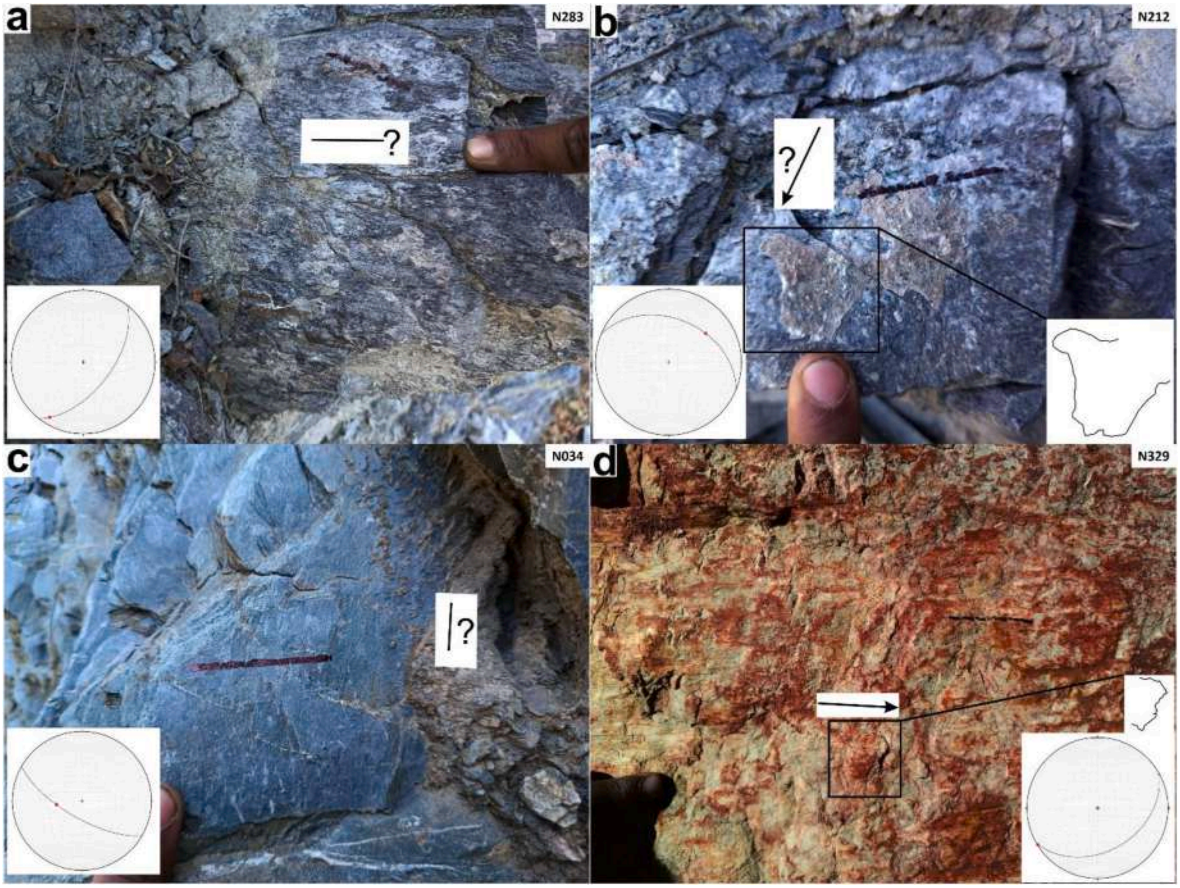

Fig. 7. Examples from K3 zone. Great circles in the stereoplot: fault plane. Red dot on the great circles: lineations developed on the fault planes. Arrow: slip direction of the missing block. ?: doubtful slip direction of missing block **a.** Moderately visible lineation, can be called slickenlines (as per Twiss and Moores, 2006), quartzite rock, Damtha Group, **b.** Probable lineation- ST5 (as per Doblas, 1998) and slickolite planes (as per Twiss and Moores, 2006), dolomite, Damtha Group, **c.** Probable lineation, dolomite, Damtha Group. **d.** Moderately visible lineation, ST5 (as per Doblas, 1998) and slickolite planes (as per Twiss and Moores, 2006), quartzite rock, Damtha Group.

Table 6
Morphometric results of sub-watersheds and main watershed of the Bhagirathi River section. Parameters (R_c, F_f, AF, HI, T, R_h and B_s) were used for TOPSIS analysis.

S-WS	Area (km^2)	Perimeter (km)	D_D (km/km^2)	D_t (km^{-1})	R_e (unitless)	R_c (unitless)	F_f (unitless)	AF (unitless)	HI (unitless)	T (unitless)	R_h (unitless)	B_s (unitless)
1	710	135	0.40	0.67	0.41	0.49	0.52	8.65	0.55	0.27	0.06	1.07
2	614	126	0.42	0.61	0.42	0.49	0.55	3.14	0.56	0.01	0.09	0.97
3	248	81	0.38	0.34	0.37	0.46	0.44	12.18	0.61	0.53	0.1	2.14
4	153	58	0.52	0.48	0.38	0.57	0.44	15.69	0.55	0.31	0.15	1.43
5	97	44	0.51	0.39	0.35	0.63	0.68	9.63	0.57	0.38	0.19	1.54
6	91	54	0.33	0.17	0.28	0.39	0.24	14.42	0.61	0.28	0.22	1.56
7	172	66	0.33	0.29	0.28	0.50	0.25	15.46	0.61	0.38	0.14	1.47
8	173	66	0.30	0.35	0.31	0.50	0.30	2.81	0.58	0.22	0.17	1.7
9	92	41	0.35	0.37	0.37	0.69	0.42	12.55	0.52	0.82	0.27	1.47
10	196	70	0.37	0.39	0.29	0.50	0.26	12.57	0.47	0.23	0.15	1.38
11	196	70	0.48	0.44	0.28	0.50	0.25	6.28	0.45	0.24	0.21	1.77
12	1458	237	0.40	0.88	0.22	0.33	0.15	8.28	0.32	0.52	0.08	2.36
13	181	66	0.39	0.44	0.37	0.52	0.43	16.06	0.42	0.64	0.11	1.03
14	92	47	0.37	0.28	0.32	0.52	0.32	13.01	0.42	0.2	0.11	1.57
15	46	32	0.43	0.16	0.36	0.56	0.40	4.89	0.55	0.48	0.21	1.45
16	262	85	0.44	0.48	0.27	0.46	0.24	2.41	0.45	0.02	0.09	2.46
17	109	56	0.45	0.30	0.28	0.44	0.25	28.01	0.47	0.51	0.12	3.35
18	80	41	0.42	0.29	0.33	0.60	0.35	3.54	0.46	0.42	0.14	1.59
19	68	34	0.39	0.21	0.42	0.74	0.54	19.32	0.42	0.41	0.14	1.47
20	80	41	0.42	0.37	0.31	0.60	0.31	11.73	0.52	0.42	0.22	1.09
21	89	50	0.38	0.24	0.25	0.45	0.20	5.39	0.52	0.19	0.22	2.83
Main watershed	7647	588	0.41	0.05	0.42	0.28	0.14	7.72	0.45	0.43	0.04	2.86

Table 7
Ranking of sub-watershed's master streams based on R^2 model. Bold numbers-highest values of R^2 in the respective rows.

Sub-Basin	Linear (unitless)	Exponential (unitless)	Logarithmic (unitless)	Power (unitless)	Difference between maximum R^2 and Linear R^2 (unitless)	Rank
1	0.9918	**0.9921**	0.8345	0.8051	0.0003	2
2	0.9891	**0.9902**	0.7281	0.6906	0.0011	3
3	**0.9915**	0.9897	0.742	0.7141	0	1
4	**0.9906**	0.9877	0.7492	0.7195	0	1
5	**0.9937**	0.9893	0.7634	0.731	0	1
6	**0.9617**	0.934	0.6692	0.6059	0	1
7	**0.9756**	0.9495	0.7957	0.7324	0	1
8	**0.9956**	0.9889	0.7874	0.7266	0	1
9	0.9841	**0.9957**	0.8506	0.7985	0.0116	7
10	0.9862	**0.9937**	0.7787	0.6945	0.0075	5
11	0.983	**0.9961**	0.8495	0.7803	0.0131	8
12	**0.9963**	0.995	0.9221	0.7968	0	1
13	0.9818	**0.9929**	0.874	0.8185	0.0111	6
14	0.9073	**0.9701**	0.9282	0.847	0.0628	11
15	0.9879	**0.9892**	0.7824	0.704	0.0013	4
16	0.9585	**0.9904**	0.8852	0.7737	0.0319	9
17	**0.9929**	0.9929	0.8806	0.8205	0	1
18	0.9176	0.9746	0.8942	0.8228	0.057	10
19	**0.9838**	0.9798	0.802	0.7431	0	1
20	**0.9506**	0.9309	0.5775	0.5458	0	1
21	**0.9489**	0.8919	0.5889	0.504	0	1

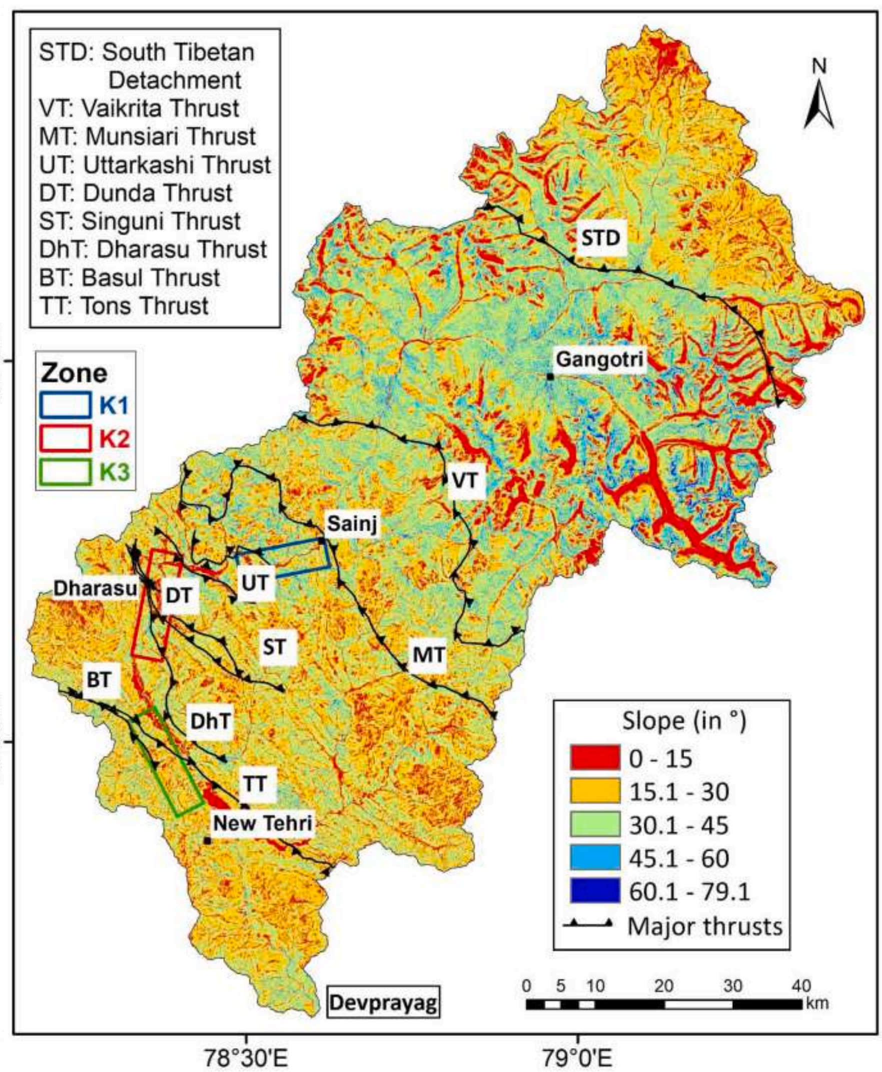

Fig. 8. Slope map of the study area. Note- STD first acted as a thrust and then as a normal fault.

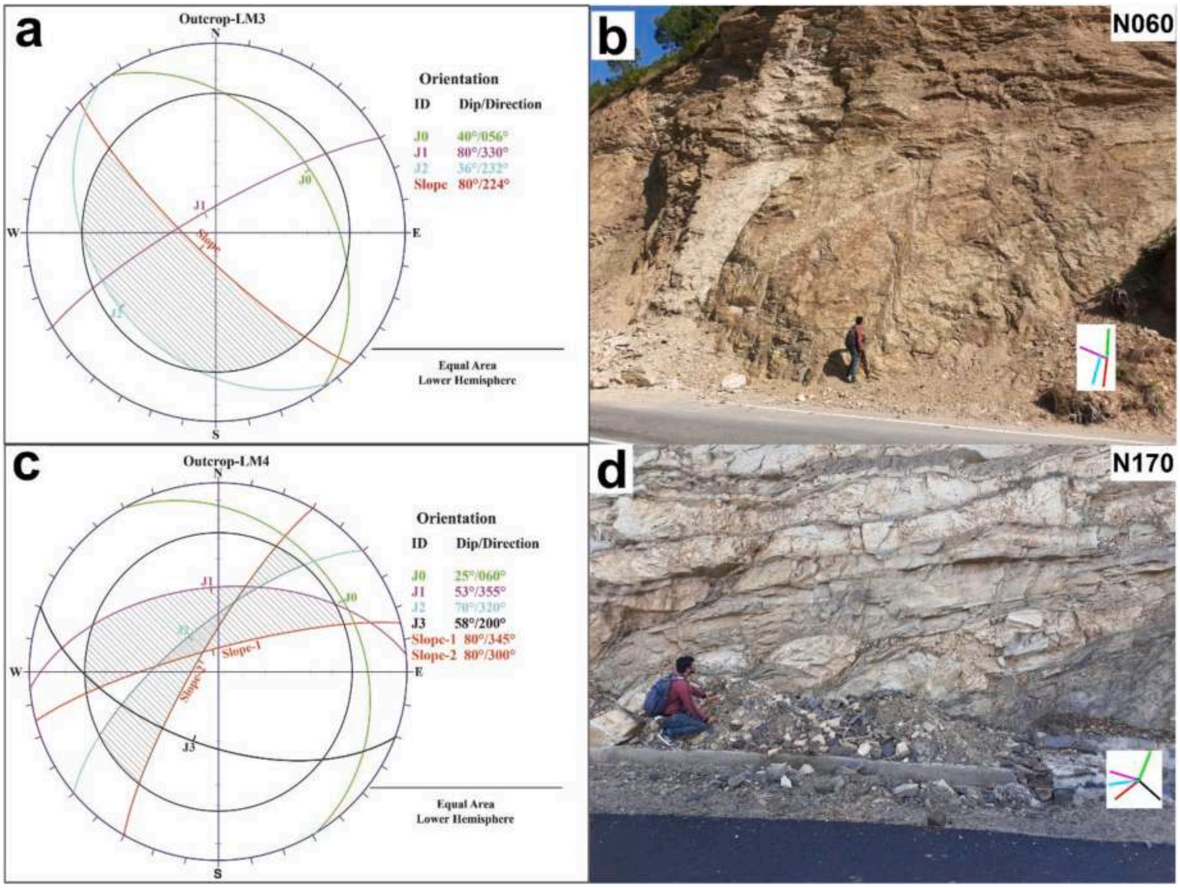

Fig. 9. Foliation plane (J0) is shown by green colour, Joint plane 1 (J1): Violet colour, Joint plane 2 (J2): Cyan colour, Joint Plane 3 (J3): Black colour, Slope: Red colour. x/y: slope direction in degree, and slope in degree. Circles in stereoplots are drawn based on the friction angle of the rock mass, which was calculated by rock mass rating. In shaded regions: hatching-planar failure, and cross hatching-wedge failure. **a.** Stereographic projection of the discontinuities at location LM-3 (near Chamba town, not falling inside K1-3 zones). Kinematic analysis shows planar failure with J2. **b.** Location – LM3 (near Chamba town, not falling inside K1-3 zones), Slightly to moderately weathered slate, slope orientation- 224/80, Ashish Kaushik marker, height 170 cm. **c.** Stereographic projection of the discontinuities at LM4 (near K3 zone). Kinematic analysis shows planar failure with J1 and J2. **d.** Location – LM4 (near K3 zone). Slightly weathered slate interbedded with quartzite, slope orientation- 345/80 and 300/80, Ashish Kaushik as marker, in sitting position height ~ 100 cm.

Based on the frequency of the occurrence of the fault planes, the study area was divided into three zones: K1, K2 and K3 (Figs. 1 and 4). The stress tensors were determined for the individual zones based on the slip movement. The strike-slip movement was only recorded from the K2 zone.

From MCT in the north up to UT in the south is classified as zone K1. Numerous normal and reverse faults were documented from here. A total of 45 normal fault planes reveals pure extension (stress regime index = 0.48) with parameters $\sigma1 = 78°/342°$, $\sigma2 = 07°/105°$, and $\sigma3 = 10°/196°$ with an NNE-SSW direction of maximum extension (Fig. 12a). Reverse movements from this area are recorded from 42 data-points denoting a pure compressional regime with a stress regime index of 2.32 (Table 10). A NE-SW compression with parameters $\sigma1 = 09°/210°$, $\sigma2 = 08°/301°$, and $\sigma3 = 78°/072°$ (Fig. 12b).

Zone K2 covers an area from the DT towards the north up to the DhT towards the south. The zone has several mesoscale normal and reverse faults. This area records strike-slip movements, which were not found in other zones (K1 and K3) (Table 10). Three tensors were determined from this zone. With 93 normal slip data points the area falls under an extensive stress regime (stress index = 0.3) with a minor radial component (Fig. 13a). The orientations of the principal stress axes are $\sigma1 = 78°/342°$, $\sigma2 = 09°/118°$, and $\sigma3 = 08°/209°$ with a NNE-SSW direction of maximum extension. A similar exercise was carried out with the 87 reverse slip data. We deduced $\sigma1 = 04°/51°$, $\sigma2 = 11°/320°$, and $\sigma3 = 78°/162°$, and the stress regime indicates compression with a radial component (stress index = 2.75) denoting a NE-SW direction of maximum compression (Fig. 13b). A pure strike-slip tensor is characterized by $\sigma1 = 10°/023°$, $\sigma2 = 77°/240°$, and $\sigma3 = 07°/115°$ with NNE-SSW shortening direction and WWN-SSE direction of maximum extension (stress index = 1.48) (Fig. 13c).

From south of the DhT up to New Tehri (Fig. 1), Tons Thrust (TT) crosses the zone K3. Only a few slips were documented from this zone (Table 10). The first tensor was calculated from just six data that indicate a pure extensive regime with parameters $\sigma1 = 73°/314°$, $\sigma2 = 14°/098°$, and $\sigma3 = 09°/191°$ (Fig. 14a). The direction of extension is NNE-SSW with a stress index of 0.55. Only four reverse movements reveal the orientation of the second tensor, $\sigma1 = 10°/250°$, $\sigma2 = 02°/340°$, and $\sigma3 = 80°/080°$ with an NE-SW direction of maximum compression, and a stress index of 2.5 (Fig. 14b). Less abundance of data makes the results less reliable, yet it is consistent with the earlier results that were observed in zone K2 and K1.

5. Discussions

Due to Bhagirathi River's tilt towards NW, its principal tributaries pour into its left bank. However, as a result of geologic and structural influences, the main watershed and the sub-watersheds display varying levels of asymmetry. The tilt angle has frequently followed the local gradient of the terrain. As per the TOPSIS analysis, S-WSs 3, 9, 12, and 17 is presently most active tectonically, while S-WSs 1, 2, 8, and 16

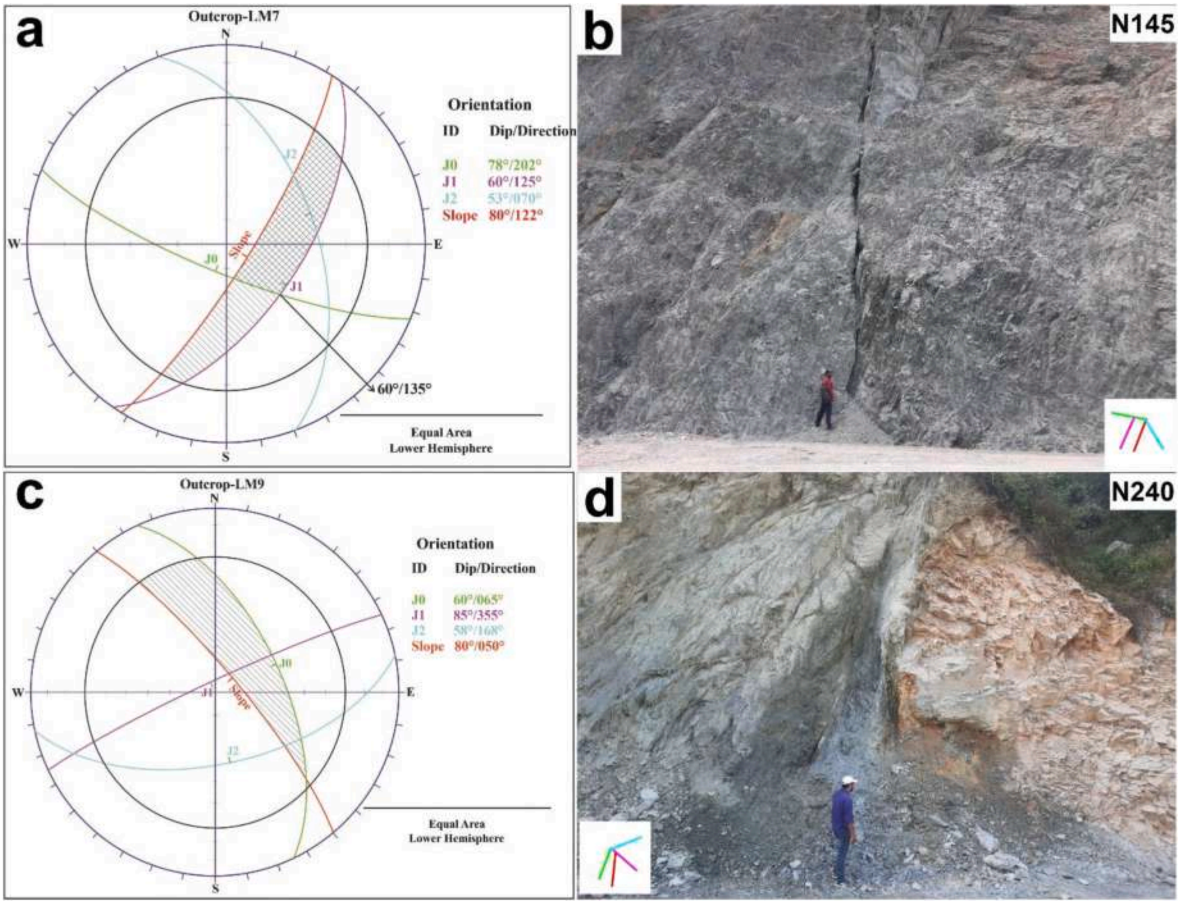

Fig. 10. Foliation plane (J0) is shown by green colour, Joint plane 1 (J1): Violet colour, Joint plane 2 (J2): Cyan colour, Slope: Red colour. x/y: slope direction in degree, and slope in degree. Circles in stereoplots are drawn based on the friction angle of the rock mass, which was calculated by rock mass rating. In shaded regions: hatching-planar failure, and cross hatching-wedge failure. **a.** Stereographic projection of the discontinuities present at location LM-7 (K3 zone) and kinematic analysis shows planar failure with J1 and wedge failure between foliation/bedding plane (J0) and J1 in N135. **b.** Location – LM-7 (K3 zone), slightly weathered quartzite, slope orientation- 122/80, Ashish Kaushik as marker, height 170 cm. **c.** Stereographic projection of the discontinuities present at location LM-9 (K2 zone) and kinematic analysis shows planar failure with J0. **d.** Location – LM9 (K2 zone), slightly to moderately weathered quartzite, slope orientation- 050/80. Ashish Kaushik as marker, height 170 cm.

Table 8
Geotechnical investigation data and rock mass classification from the study area. Refer Fig. 4b for the locations LM-1 to 10.

Location	Rock Type	RQD (%)	RMR (unitless)	Class	Type of failure	SMR (unitless)	Slope condition	Failure Probability (unitless)
LM-1	Quartzite	45	48–52	III	Wedge	14	Very bad	0.9
LM-2	Slate and quartzite interbedded	38	48–59	III	Wedge	11	Very bad	0.9
LM-3	slate	25	42–52	III	Planar	12	Very bad	0.9
LM-4	Slate and quartzite interbedded	45	45–57	III	Planar	17	Very bad	0.9
LM-5	Quartzite	47	43–59	III	N/A	42	Normal	0.4
LM-6	Phyllite	25	40–53	III	Planar	37	Bad	0.6
LM-7	Quartzite	47	46–59	III	Planar & wedge	18	Very bad	0.9
LM-8	Quartzite	55	49–64	II-III	N/A	50	Normal	0.4
LM-9	Phyllite, quartzite and dolerite contact	37	42–59	III	Planar	16	Very bad	0.9
LM-10A	Dolerite	45	46–54	III	Planar & wedge	7	Very bad	0.9
LM-10B	Phyllite	25	39–53	II-III	Planar & wedge	12	Very bad	0.9

exhibits the least activity (Table 11). The maximum value of HI = 0.61 is obtained for S-WSs 6 and 7, indicating a youthful and less eroded area. The lowest value of HI = 0.32 is found for S-WS 12, suggesting old and more eroded areas with dissected drainage basins.

The SL value for the master stream of S-WS 17 is maximum at ~ 23 km from its source of origin, near the village Chinyalisaur. Simultaneously, SL value for master stream of S-WS 16 is maximum at ~ 31 km from its source of origin, near Pandla Bugyal. Higher SL values in S-WS 17 are also documented, where lineaments, TT and BT cross. Higher SL is noted from the S-WS 16 where ST and lineaments in Nagthat Formation occur. SL indices of master streams of all the sub-watersheds are presented in Repository R6.

The main channel of Bhagirathi is comparatively active as it is under class 2 (0.35–0.50) and is in a high active zone as per TOPSIS analysis. Generally speaking, the TH is less tectonically active at present than the HH and LH. Even within a single unit of the Himalaya, such as within the

Table 9
Lab testing results for soil samples.

Location	Cohesion (kg cm^{-2})	Friction angle (°)	Soil type	Natural moisture content (%)
L1	0.2	4.52	Gravely silty sand	11.9
L2	0.13	23.36	Silty clayey	6
L3	–	–	Gravely sand	4.9
L4	0.36	17.64	Gravely sand	6.8
L5A	0.35	6.39	Gravely sand	10.3
L5B	0.43	30.46	Gravely sand	8.2
L6	0.5	25.45	Gravely sand	3.4
L7	0.55	2.41	Gravely sand	7.2
L8	0.54	16.49	Gravely silty sand	5.3
L9	–	–	Gravely silty sand	7
L10	0.57	15.43	Gravely sand	4.9
L11	0.81	6.73	Gravely sand	6.7
L12	0.56	20.81	Gravely sand	5.4
L13	–	–	Sandy gravel	5.6
L14	0.76	4.4	Gravely sand	5.1
L15	0.57	5.37	Gravely silty sand	5.8
L16	–	–	Gravely silty sand	7.4
L17	0.05	35.26	Gravely sand	5.1
L18	0.83	5.43	Gravely sand	5.9
L19	0.52	12.9	Gravely sand	5.4
L20	0.49	13.17	Gravely sand	6.6
L21	0.31	13.22	Gravely sand	9.4
L22	0.22	6.33	Gravely sand	8
L23	0.5	8.03	Gravely sand	8

Table 10
Paleostress analysis results of normal, reverse, and strike-slip movements recorded from the study area.

Zones	Sense of slip	σ1 (°/°)	σ2 (°/°)	σ3 (°/°)	$R^{\prime}$ (stress Index, unitless)	Direction of maximum compression	Direction of maximum extension	Fig.
K1-3	Normal	83/302	06/103	02/193	0.25	–	NNE-SSW	11a
	Reverse	01/030	05/300	85/135	2.69	NE-SW	–	11b
	Strike-slip	10/023	77/240	07/115	1.48	NNE-SSW	WWN-SSE	11c
K1	Normal	78/342	07/105	10/196	0.48	–	NNE-SSW	12a
	Reverse	09/210	08/301	78/072	2.32	NE-SW	–	12b
K2	Normal	78/342	09/118	08/209	0.3	–	NNE-SSW	13a
	Reverse	04/51	11/320	78/162	2.75	NE-SW	–	13b
	Strike-slip	10/023	77/240	07/115	1.48	NNE-SSW	WWN-SSE	13c
K3	Normal	73/314	14/098	09/191	0.55	–	NNE-SSW	14a
	Reverse	10/250	02/340	80/080	2.5	NE-SW	–	14b

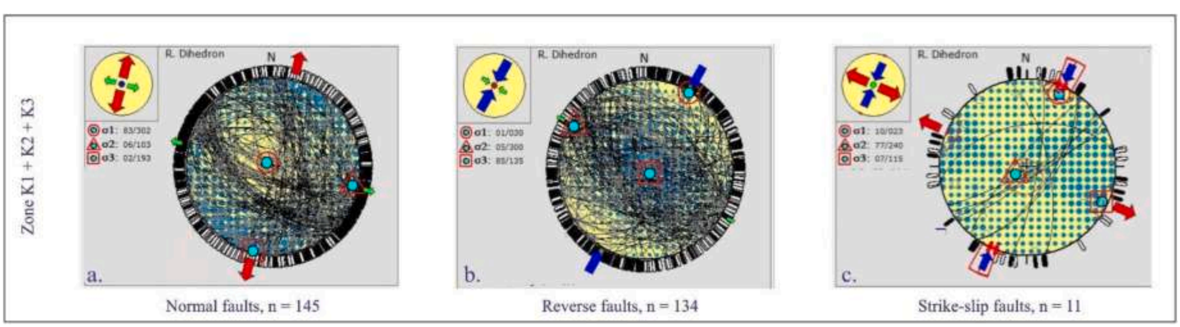

Fig. 11. Paleostress results for faults collected from K1, K2 and K3 zones using the Right Dihedron Method in the WinTensor software (ver. 5.8.8). The extensive stress tensor is represented by large red arrows. **(a)**, while the large blue arrows indicate a compressive stress regime **(b)**. Small green arrows represent a radial component (a and b), and when the blue and red arrows are of similar size, it implies a Strike-slip stress regime **(c)**. The orientation (dip/dip direction) of σ1, σ2, and σ3 are illustrated by a circle, triangle, and square respectively within the stereo plot, with a summary provided on the left-hand side of each diagram. 'n' represents the number of fault data used to generate the diagram. **a.** A total of 145 normal faults data reveals an extension towards 13°–193° with a stress index (Delvaux et al., 1997) $R^{\prime} = 0.25$. **b.** In the case of reverse faults, the direction of compression is along 30°–210°, with the stress index value $R^{\prime} = 2.69$. **c.** An overall pure strike-slip movement was observed in the study area with the stress index value $R^{\prime} = 1.48$.

HH there are zones (e.g., S-WS 8 and 9) of different intensities of tectonic activities (Fig. 2).

In the study area, the available earthquake data do not show preferential cluster around thrusts (Fig. 15). Stability analysis of few slopes show planar and wedge type of failures. Lab testing of soil samples show less cohesion value at most of the places, which can be due to the sandy type of soil in nature intermixed with pebbles.

STD passes from two watershed of the different intensities of tectonically active zones: S-WS 3 (TOPSIS value 0.589, unitless) and S-WS 2 (TOPSIS value 0.115, unitless) (Fig. 2). DhT and ST also pass

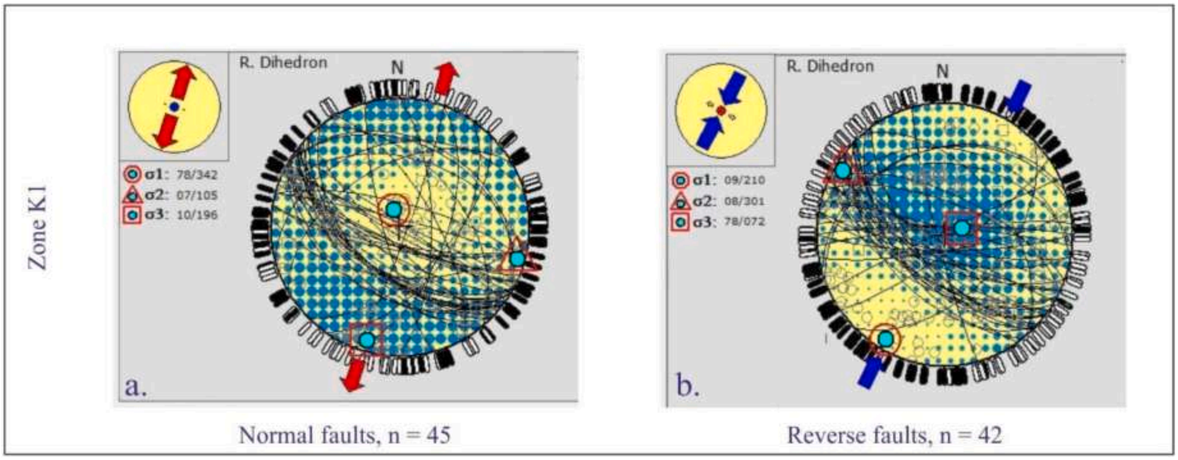

Fig. 12. Paleostress analysis from the K1 zone. Red arrow: extension; blue arrow: compression; small green arrows: radial movements. The orientation (dip/dip direction) of σ1, σ2, and σ3 are illustrated by a circle, a triangle and a square, respectively. 'n': number of fault data. **a.** 45 normal faults data reveal a pure extension along 16°–196° with a stress index (Delvaux et al., 1997) R′ = 0.48. **b.** In the case of reverse faults, the direction of pure compression is 30°–210°, with R′ = 2.32.

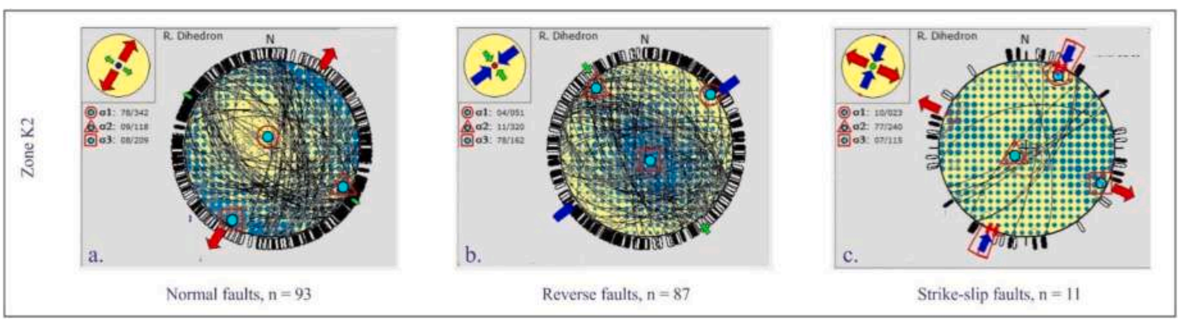

Fig. 13. Paleostress analysis from the K2 zone. Red arrow: extension; blue arrow: compression; small green arrows: radial components. The orientation (dip/dip direction) of σ1, σ2, and σ3 are illustrated by a circle, a triangle and a square, respectively. 'n': number of fault data. **a.** A total of 95 normal faults data reveals an extension towards 16°–196° with a stress index (Delvaux et al., 1997) R′ = 0.3. **b.** In the case of reverse faults, the direction of compression is along 51°–231°, with R′ = 2.75. **c.** An overall pure strike-slip movement was observed in the study area with R′ = 1.48.

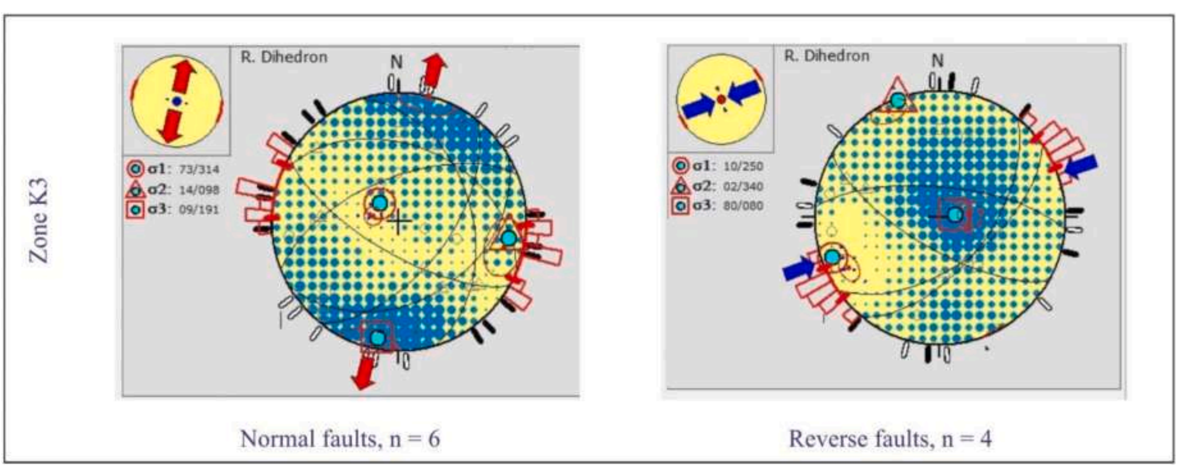

Fig. 14. Paleostress analysis from the K3 zone. The Right Dihedron Method was used in the WinTensor software (ver. 5.8.8) to obtain the results. The abundance of the fault plane drops in this area which makes the paleostress results less reliable. Red arrow: extension; blue arrow: compression; small green arrows: radial components. The orientation (dip/dip direction) of σ1, σ2, and σ3 are illustrated by a circle, a triangle and a square, respectively. 'n': number of fault data. **a.** A total of 6 normal faults data reveals a pure extension towards 11°–191° with a stress index (Delvaux et al., 1997) R′ = 0.55. **b.** In the case of reverse faults, the direction of pure compression is 70°–250°, with the stress index value R′ = 2.5.

Table 11
Tectonically active ranges for S-WSs based on the TOPSIS analysis.

Magnitude	TOPSIS range (unitless)	S-WS/WS
Very high	0.5–1	3, 9, 12, 17
High	0.35–0.50	4, 5, 6, 7, 13, 18, 19, 20, 21, main watershed
Moderate	0.25–0.34	10, 11, 14, 15
Low	<0.25	1, 2, 8, 16

through different intensities of tectonically active zones: S-WS 14 (TOPSIS value 0.308, unitless) and S-WS 16 (TOPSIS value 0.072, unitless) (Fig. 2). This can indicate that these thrusts could be variably active at present along their trend. Interestingly variable degree of activity along the same fault trend has been established from other study areas worldwide (e.g., Kelley et al., 2013).

The K2 zone is highly active tectonically at present. Soil sample analysis also show less cohesion values. Matli, Dilsaur, Nakuri, Athali, Veerpur, Dunda Nalupani, Dharasu etc. are the few villages situated in K2 zone where the inhabitants can be affected by natural disasters

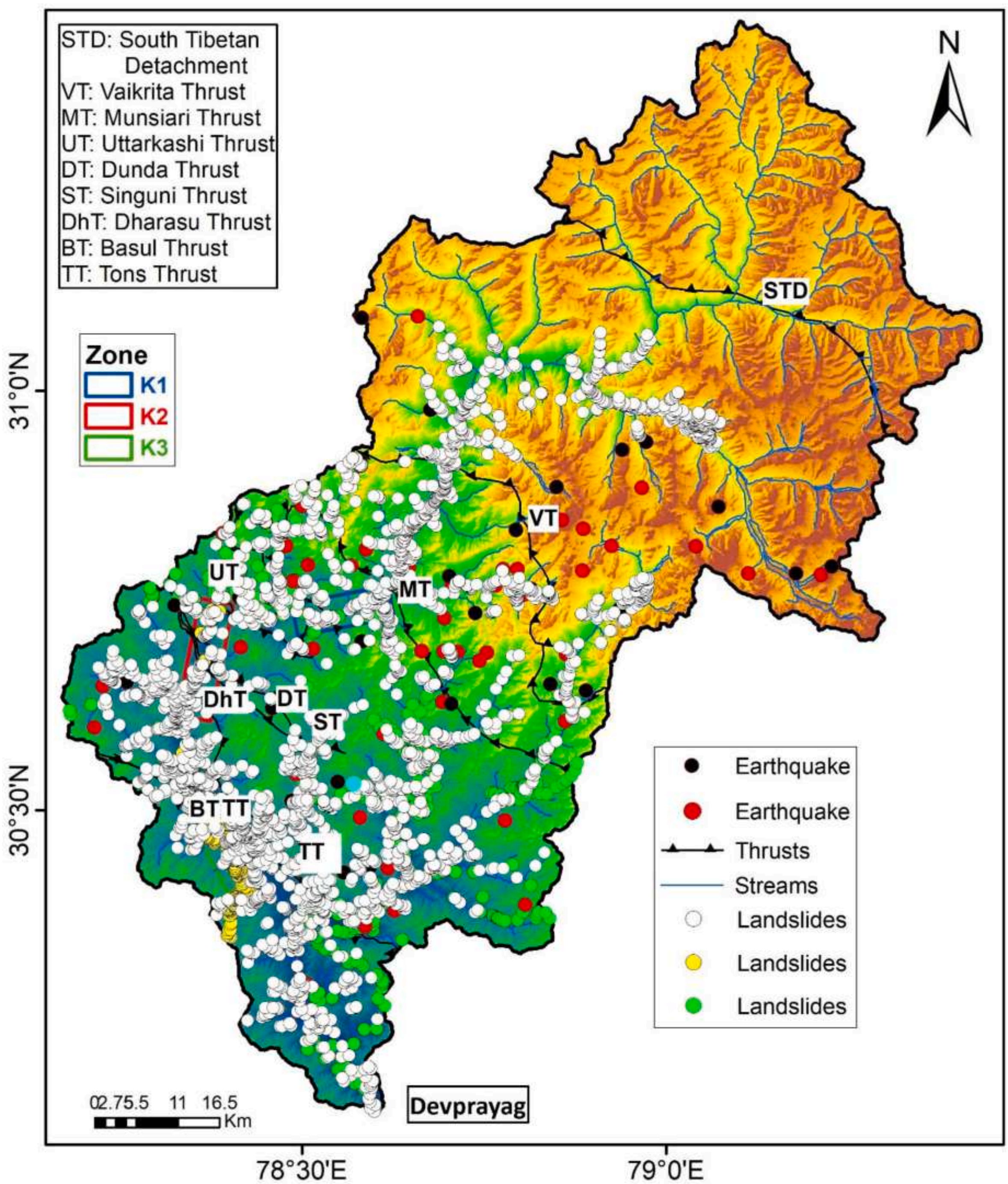

Fig. 15. Landslide and earthquake location map of the study area. Seismicity data has been taken from Geological Survey of India (1963–2023) (Internet reference 2) shown in red circles and USGS (1948–2023) (Internet reference 7) shown in black circles. Landslide points shown in green circles, yellow circles (from 2012 to 2023) and white circles are reproduced from Internet reference 8; Internet reference 9 and Bhambri et al. (2017), respectively.

(Repository R7). Slope stability issues in the K2 zone will require detail study in the context of structural geology.

6. Conclusions

The DhT and ST are tectonically active with varying intensity along their lengths. BT, DhT, TT, ST, MT, VT and STD seem to have variable tectonic activity at present along their lengths. Overall, the main WS of the Bhagirathi river is in a tectonically highly active zone.

RMR indicates that the rock mass condition in the studied rocks in the LH is of fair quality. The rock mass's SMR suggest that the majority of slopes in this area are (entirely) unstable, which can create a significant hazard. Based on the slope stability analysis, it has been determined that out of the 11 places analyzed, nine are prone to failure due to poor rock mass conditions. Unfavourable orientation of discontinuities and low cohesion within the Lesser Himalayan portion in the K2 and the K3 zones have been documented.

Paleostress analysis indicates two stress regimes in the LH over the geologic time: *(i)* NE-SW extension ($\sigma1 = 83^\circ/302^\circ$, $\sigma2 = 06^\circ/103^\circ$ and $\sigma3 = 02^\circ/193^\circ$, $R^{/} = 0.25$) that created normal faulting, *(ii)* NNE-SSW compression ($\sigma1 = 01^\circ/030^\circ$, $\sigma2 = 05^\circ/300^\circ$, $\sigma3 = 85^\circ/135^\circ$, $R^{/} = 2.5$) created reverse faulting in K1, K2 and K3 zones. No distinct cross-cut relationship was observed amongst strike-slip, normal and reverse faults. The strike-slip regime probably prevailed in the region as a part of the oblique component of normal or reverse movement to accommodate arc-parallel shear along the obliquely converging Indian plate $\sim$ 55 Ma onward.

CRediT authorship contribution statement

Nikhil Puniya: Writing – original draft, Software, Investigation, Formal analysis. **Soumyajit Mukherjee:** Writing – review & editing, Writing – original draft, Supervision, Investigation, Conceptualization. **Atul Kumar Patidar:** Writing – review & editing, Supervision, Project administration. **Mohit Kumar Puniya:** Investigation. **Mery Biswas:** Writing – original draft, Supervision, Investigation, Formal analysis. **Tuhin Biswas:** Writing – original draft, Investigation.

Declaration of competing interest

Authors do not have conflict of interest with anyone regarding this research work.

Acknowledgements

NP and AKP acknowledge UPES for providing research fellowship and infrastructures. Guddu Singh (UPES) assisted in soil sample analysis. Thanks to Ashish Kaushik (Kurukshetra University) and Vimal Puniya for the support during field work. SM thanks internal grant of IIT Bombay. Adrija Raha (Presidency University, Kolkata) and Ankita Paul (JIS University) are thanked for providing internal review comments. Chief Editor Ian Alsop, and two reviewers (Victor Alania and anonymous) provided detail comments. Thanks to the Managing Editor Lorna Alsop. Maps of landslides, mainly from the Geological Survey of India, from the study area are presented as Repository 8.

Appendix A. Supplementary data

Supplementary data to this article can be found online at https://doi.org/10.1016/j.jsg.2024.105288.

Abbreviations

AF	Asymmetric Factor
AHP	Analytical hierarchy process
Bl	Length between headwater to the mouth of the basin
Bs	Basin shape
Bw	Width at widest point of the basin
BT	Basul Thrust
CF	Collaborative filtering
Da	Distance from drainage
Dd	Distance from basin midline to basin divide
D_D	Drainage density
DEM	Digital elevation model
DhT	Dharasu Thrust
DST	Direct Shear Test
Dt	Drainage texture
DT	Dunda Thrust
Ff	Form Factor
GIS	Geographic information system
GPS	Global Positioning System
GSI	Geological Survey of India
HH	Higher Himalaya
HI	Hypsometric integral
IAT	Index of active tectonics
ILH	Inner Lesser Himalaya
ISRM	International Society of Rock Mechanics
J0	Foliation or bedding plane
J1	Joint plane 1
J2	Joint plane 2
J3	Joint plane 3
LH	Lesser Himalaya
LHI	Landslide Hazard Index

LISS II	Linear Imaging Self Scanning Sensor
Lb	Stream length
Lu	Cumulative stream length
Lur	Stream length ratio
MBT	Main Boundary Thrust
MCDA	Multi criteria decision analysis
MCDM	Multi criteria decision making
MCT	Main Central Thrust
MFT	Main Frontal Thrust
MIO	Multi-index overlay
MT	Munsiari Thrust
M-TOPSIS	Multi-Objective Optimization on the Basis of Ratio Analysis
NIS	Negative Ideal Solution
Nu	Stream number
OLH	Outer Lesser Himalaya
P-A	Production-area
PCA	Principal component analysis
PIS	Positive Ideal Solution
Rc	Circularity ratio
Re	Elongation ratio
Rh	Relief ratio
RMR	Rock mass rating
RQD	Rock quality designation
RT	Ramgarh Thrust
SAW	Simple Additive Weighting
SH	Sub-Himalaya
SI	Sinuosity Index
SL	Stream length
SMR	Slope mass rating
SPIM	Stream Power Incision Model
SRTM	Shuttle Radar Topography Mission
ST	Singuni Thrust
STD	South Tibetan Detachment
Su	Stream order
Suf	1st order stream
S-WS	Sub-watershed
TOPSIS	Technique for Order Preference by Similarity to Ideal Solution
TT	Tons Thrust
UCS	Uniaxial Compressive Strength
USGS	United States Geological Survey
UT	Uttarkashi Thrust
VIKOR	VlseKriterijumska Optimizacija I Kompromisno Resenje
VT	Vaikrita Thrust
WS	Watershed
XRD	X-ray diffraction

Symbols

A_1	Angle between joint strikes and slope orientation
Bj	Joint dip angle in planar failure
A+	Positive ideal
A	Negative ideal
Ci+	Relative closeness to the ideal solution
F_1, F_2, F_3, F_4	Paremeters/factors used in eqns 7 to 9
J	Positive criteria
J'	Negative criteria
n_{ij}	Normalized decision matrix
R'	Stress Index
Si+	Separation from positive ideal solution
Si	Separation from negative ideal solution
σ1	Maximum principal stress
σ2	Intermediate principal stress
σ3	Minimum principal stress
T	Transverse topographic symmetry factor
V+	Ideal best
V	Ideal worst

V_{ij} Weighted normalized matrix
Wj Weight calculated by analytical hierarchy process
X_{ij} Rating of alternative with respect to criteria

Software used in this article-

Software	Version	Year
ArcGIS	10.8	2020
Microsoft Excel	Microsoft 365	2024
Stereonet	11.6.0	2024
WinTensor	5.8.8	2018

Data availability

Data will be made available on request.

References

Agarwal, N.C., Kumar, G., 1973. Geology of the upper Bhagirathi and Yamuna valleys, Uttarkashi district, Kumaun Himalaya. Himal. Geol. 3, 2–23.

Ahmad, S., Khan, K., 2020. Impact of elevation - Glaciation - tectonics on landscape characteristics of the watersheds in Bhagirathi valley, Garhwal Himalaya. J. Indian Assoc. Sedimentol. 37, 141–147. https://doi.org/10.51710/jias.v37i2.110.

Al-Attar, Z.T., Othman, A.A., Al-Hakari, S.H.S., Obaid, A.K., Salar, S.G., Liesenberg, V., 2022. A neotectonic statistical assessment through watershed geomorphic analysis: a case study in the Greater Zab River Basin, Turkey–Iraq. Environ. Earth Sci. 81, 355. https://doi.org/10.1007/s12665-022-10478-7.

Angelier, J., 1994. Fault slip analysis and paleostress reconstruction. Continental Deformation. Pergamon Press, Oxford, pp. 53–100.

Aouragh, M.H., Essahlaoui, A., 2018. A TOPSIS approach-based morphometric analysis for sub-watersheds prioritization of high Oum Er-Rbia basin, Morocco. Spatial Infor. Res. 26, 187–202. https://doi.org/10.1007/s41324-018-0169-z.

Bahroudi, A., Ferdowsi, H., Moradzadeh, A., Abedi, M., 2023. TOPSIS vs MIO: applications to gold prospectivity mapping; a case study of the Basiran-Mokhtaran Area- Eastern Iran. Int. J. Min. Geol. Eng. 58, 69–87, 10.10.22059/IJMGE.2023.367734.595119.

Bali, R., Awasthi, D.D., Tiwari, N.K., 2003. Neotectonic Control on the geomorphic evolution of the Gangotri glacier valley, Garhwal Himalaya. Gondwana Res. 6, 829–838. https://doi.org/10.1016/S1342-937X(05)71028-5.

Ballabh, H., Pillay, S., Negi, G.C.S., Pillay, K., 2014. Relationship between selected Physiographic features and landslide occurrence around four hydropower projects in Bhagirathi valley of Uttarakhand, western Himalaya, India. Int. J. Geosci. 5, 1088–1099. https://doi.org/10.4236/ijg.2014.510093.

Barman, B.K., Bawri, G.R., Rao, K.S., Singh, S.K., Patel, D., 2020. Drainage network analysis to understand the morphotectonic significance in upper Tuirial watershed, Aizawl, Mizoram. In: Agricultural Water Management: Theories and Practices. Elsevier, pp. 349–373. https://doi.org/10.1016/B978-0-12-812362-1.00017-5.

Barman, B.K., Rao, C.U.B., Rao, K.S., Patel, A., Kushwaha, K., Singh, S.K., 2021. Geomorphic analysis, morphometric-based prioritization and tectonic implications in Chite Lui River, Northeast India. J. Geol. Soc. India 97, 385–395. https://doi.org/10.1007/s12594-021-1696-0.

Bhambri, R., Mehta, M., Singh, S., Jayangondaperumal, R., Gupta, A.K., Srivastava, P., 2017. Landslide inventory and damage assessment in the Bhagirathi valley, Uttarakhand, during June 2013 flood. Himal. Geol. 38, 193–205.

Bhargava, O.N., Singh, B.P., 2020. Geological evolution of the Tethys Himalaya. Episodes J. Int. Geosci. 43, 404–416.

Bhattacharjee, D., 2015. Morphological characteristics of Gangotri glacier area, Uttarakhand using GIS & Remote Sensing techniques. Am. Int. J. Res. Humanit. Arts Soc. Sci. AIJRHASS 15–509. May. http://www.iasir.net.

Bieniawski, Z.T., 1989. Engineering Rock Mass Classifications: a Complete Manual for Engineers and Geologists in Mining, Civil, and Petroleum Engineering, first ed. Wiley, New York. ISBN: 978-0471601722.

Biswas, M., Paul, A., Jamal, M., 2021. Tectonics and channel morpho-hydrology—a quantitative discussion based on secondary data and field investigation, pp. 461–494. https://doi.org/10.1007/978-3-030-60143-0_16.

Biswas, T., Bose, N., Dutta, D., Mukherjee, S., 2022. Arc-parallel shears in collisional orogens: global review and paleostress analyses from the NW Lesser Himalayan Sequence (Garhwal region, Uttarakhand, India). Mar. Petrol. Geol. 138, 105530. https://doi.org/10.1016/j.marpetgeo.2022.105530.

Biswas, B., Ghosh, A., Sailo, B.L., 2023. Spring water suitable and vulnerable watershed demarcation using AHP-TOPSIS and AHP-VIKOR models: study on Aizawl district of North-Eastern hilly state of Mizoram, India. Environ. Earth Sci. 82, 80. https://doi.org/10.1007/s12665-023-10766-w.

Bose, N., Mukherjee, S., 2019. Field documentation and genesis of the back-structures from the Garhwal lesser Himalaya, Uttarakhand, India. In: Sharma, Villa IM., Kumar, S. (Eds.), Crustal Architecture and Evolution of the Himalaya-Karakoram-Tibet Orogen, vol. 481. Geological Society of London Special Publications, pp. 111–125. https://doi.org/10.1144/SP481-2018-81.

Bose, N., Mukherjee, S., 2020. Estimation of deformation temperatures, flow stresses and strain rates from an intra-continental shear zone: the Main Boundary Thrust, NW Himalaya (Uttarakhand, India). Mar. Petrol. Geol. 112, 104094. https://doi.org/10.1016/j.marpetgeo.2019.104094.

Bott, M.H.P., 1959. The mechanics of oblique slip faulting. Geol. Mag. 96, 109–117. https://doi.org/10.1017/S0016756800059987.

Bull, W.B., McFadden, L.D., 1977. Tectonic geomorphology north and south of the garlock fault, California. In: Doehring, D.O. (Ed.), Geomorphology in Arid Regions: A Proceedings Volume of the 8th Annual Geomorphology Symposium, pp. 115–138.

Catlos, E.J., Harrison, T.M., Manning, C.E., Grove, M., Rai, S.M., Hubbard, M.S., Upreti, B.N., 2002. Records of the evolution of the Himalayan orogen from in situ Th–Pb ion microprobe dating of monazite: Eastern Nepal and western Garhwal. J. Asian Earth Sci. 20, 459–479. https://doi.org/10.1016/S1367-9120(01)00039-6.

Chakraborty, D., Anbalagan, R., 2008. Landslide hazard evaluation of road cut slopes along Uttarkashi-Bhatwari road, Uttaranchal Himalaya. J. Geol. Soc. India 71, 115–124. https://www.geosocindia.org/index.php/jgsi/article/view/80898.

Chauhan, V., Dixit, J., 2023. Geomorphic anomalies in Uttarakhand, India: a GIS-based approach for active tectonics. J. Earth Syst. Sci. 133, 2. https://doi.org/10.1007/s12040-023-02208-9.

Chen, C.-T., 2000. Extensions of the TOPSIS for group decision-making under fuzzy environment. Fuzzy Set Syst. 114, 1–9. https://doi.org/10.1016/S0165-0114(97)00377-1.

Choudhari, P.P., Nigam, G.K., Singh, S.K., Thakur, S., 2018. Morphometric based prioritization of watershed for groundwater potential of Mula river basin, Maharashtra, India. Geol. Ecol. Landsc. 2, 256–267. https://doi.org/10.1080/24749508.2018.1452482.

Cox, R.T., 1994. Analysis of drainage-basin symmetry as a rapid technique to identify areas of possible Quaternary tilt-block tectonics: an example from the Mississippi Embayment. Geol. Soc. Am. Bull. 106 (5), 571–581. https://doi.org/10.1130/0016-7606.

Das, S., Sangode, S.J., 2022. Effects of Differential Tectonic Uplift on Steepness and Concavity Indices and Erosion Rates in between the Major Thrusts in Bhagirathi-Alaknanda Catchments. NW Himalayas, India, pp. 51–66. https://doi.org/10.1007/978-3-030-95435-2_2.

Dasgupta, S., Mukherjee, S., Vanik, N., Chatterjee, R., Pal, S.K., 2023. Paleostress analyses and rift kinematics of the petroliferous Barmer rift basin, western Rajasthan, India. Mar. Petrol. Geol. 156, 106442. https://doi.org/10.1016/j.marpetgeo.2023.106442.

Delvaux, D., 1993. The TENSOR program for paleostress reconstruction: examples from the east African and the Baikal rift zones. Terra. Nova 5, 216.

Delvaux, D., Sperner, B., 2003. New aspects of tectonic stress inversion with reference to the TENSOR program. In: Nieuwland, D.A. (Ed.), New Insights into Structural Interpretation and Modeling, vol. 212. Geological Society, London, Special Publications, pp. 75–100. https://doi.org/10.1144/gsl.sp.2003.212.01.06.

Delvaux, D., Moeys, R., Stapel, G., Petite, C., Levi, K., Miroshnichenko, A., Ruzhich, V., San'kov, V., 1997. Paleostress reconstructions and geodynamics of the Baikal region, Central Asia, Part 2. Cenozoic rifting. Tectonophysics 282, 1–38.

Doblas, M., 1998. Slickenside kinematic indicators. Tectonophysics 295, 187–197. https://doi.org/10.1016/S0040-1951(98)00120-6.

Dutta, D., Mukherjee, S., 2021. Extrusion kinematics of UHP terrane in a collisional orogen: EBSD and microstructure-based approach from the Tso Morari Crystallines (Ladakh Himalaya). Tectonophysics 880, 228641. https://doi.org/10.1016/j.tecto.2020.228641.

Dzwairo, R., Singh, S.K., Patel, A., 2024. Soil erosion susceptibility assessment through morphometric analysis and morphotectonic implications in Rietspruit sub-basin, South Africa. Environ. Dev. Sustain. https://doi.org/10.1007/s10668-024-04650-1.

Evans, I.S., Hengl, T., Gorsevski, P., 2009. Chapter 22 applications in geomorphology. Dev. Soil Sci. 33, 497–525. https://doi.org/10.1016/S0166-2481(08)00022-6.

Goodman, R.E., 1989. Introduction to Rock Mechanics, second ed. John Wiley & Sons Inc. ISBN: 978-0471812005.

GSI, 2016. Landslide Compendium of Northwest Himalayas. Sp Publ 107. GSI, Kolkata. ISSN: 0254-0436.

Gupta, P., Anbalagan, R., 1997. Slope stability of Tehri Dam Reservoir Area, India, using landslide hazard zonation (LHZ) mapping. Q. J. Eng. Geol. 30, 27–36. https://doi.org/10.1144/GSL.QJEGH.1997.030.P1.03.

Gupta, R.P., Saha, A.K., Arora, M.K., Kumar, A., 2006. Landslide hazard zonation in a part of Doon valley using remote sensing and GIS. Himal. Geol. 13, 11006.
Gupta, V., Nautiyal, H., Kumar, V., Jamir, I., Tandon, R.S., 2016. Landslide hazards around Uttarkashi township, Garhwal Himalaya, after the tragic flash flood in June 2013. Nat. Hazards 80, 1689–1707. https://doi.org/10.1007/s11069-015-2048-4.
Hancock, P.L., 1985. Brittle microtectonics: principles and practice. J. Struct. Geol. 7, 437–457. https://doi.org/10.1016/0191-8141(85)90048-3.
Hare, P.W., Gardner, T.W., 1985. Geomorphic indicators of vertical neotectonism along converging plate margins, Nicoya Peninsula, Costa Rica. Tectonic Geomorphol. 4, 75–104.
Horton, R.E., 1932. Drainage-basin characteristics. Eos, Transact. Am. Geophys. Union 13 (1), 350–361. https://doi.org/10.1029/TR013i001p00350.
Horton, R.E., 1945. Erosional development of streams and their drainage basins; hydrophysical approach to quantitative morphology. GSA Bulletin 56, 275–370. https://doi.org/10.1130/0016-7606(1945)56[275:EDOSAT]2.0.CO;2.
Hwang, C.-L., Yoon, K., 1981. Multiple Attribute Decision Making, vol. 186. Springer Berlin Heidelberg. https://doi.org/10.1007/978-3-642-48318-9.
Imayama, T., Bose, N., Yi, K., Jeong, Y.-J., Horie, K., Takehara, M., Kawabata, R., 2023. Zircon U–Pb, Hf, and O isotopic constraints on the tectonic affinity of the basement of the Himalayan orogenic belt: insights from metasedimentary rocks, orthogneisses, and leucogranites in Garhwal, NW India. Precambrian Res. 397, 107183. https://doi.org/10.1016/j.precamres.2023.107183.
Internet reference 1: Lithology, 2024. Geological Survey of India. Government of India, Kolkata, India. https://bhukosh.gsi.gov.in/Bhukosh/MapViewer.aspx.
Internet reference 2: Earthquake, 2024. Geological Survey of India. Government of India, Kolkata, India. https://bhukosh.gsi.gov.in/Bhukosh/MapViewer.aspx.
Internet reference 3. https://earthexplorer.usgs.gov//;dds.cr.usgs.gov/download-staging/eyJpZCI6NjU1ODc4NjI1LCJjb250YWN0SWQiOjI2NjQ2NDI2fQ==. (Accessed 30 November 2023).
Internet reference 4: IS 2720-4, 1985. efaidnbmnnnibpcajpcglclefindmkaj. https://ia803007.us.archive.org/35/items/gov.in.is.2720.4.1985/is.2720.4.1985.pdf.
Internet reference 5: IS 2720-13, 1986. efaidnbmnnnibpcajpcglclefindmkaj. https://law.resource.org/pub/in/bis/S03/is.2720.13.1986.pdf.
Internet reference 6, 1973. efaidnbmnnnibpcajpcglclefindmkaj. IS 2720-2. https://law.resource.org/pub/in/bis/S03/is.2720.2.1973.pdf.
Internet reference 7: Earthquake. USGS. URL: https://earthquake.usgs.gov/earthquakes/map/?ex-tent=30.17125,78.26111&extent=30.55339,79.09607&timeZone=utc. (Accessed 12 October 2024).
Internet reference 8: Landslide, 2024. Geological Survey of India. Government of India, Kolkata, India. https://bhukosh.gsi.gov.in/Bhukosh/MapViewer.aspx.
Internet reference 9: Google Earth Pro 7.3.6.9796, 2024. Uttarakhand. Landslide polygons and points. Available at: https://earth.google.com/web/. (Accessed 10 September 2024).
ISRM, 2007. The Complete ISRM Suggested Methods for Rock Characterization, Testing and Monitoring: 1974-2006, first ed. International Society for Rock Mechanics. Commission on Testing Methods.
Jain, A.K., 1971. Stratigraphy and tectonics of lesser Himalayan region of Uttarkashi, Garhwal Himalaya. Himal. Geol. 1, 25–58.
Jayangondaperumal, R., Thakur, V.C., Joevivek, V., Rao, P.S., Gupta, Ak, 2018. Active tectonics of Kumaun and Garhwal Himalaya. Springer Nat. Hazards. ISBN-10: 9811341001.
Kamal, V., Sipolya, R., Kumar, R., Mukherjee, S., 2016. Morphometric and hydrological study of Alaknanda and Bhagirathi basins. In: Geostatistical and Geospatial Approaches for the Characterization of Natural Resources in the Environment. Springer International Publishing, pp. 809–815. https://doi.org/10.1007/978-3-319-18663-4_125.
Kanga, S., Meraj, G., Farooq, M., Singh, S.K., Nathawat, M.S., 2022. Disaster Management in the Complex Himalayan Terrains: Natural Hazard Management, Methodologies & Policy Implications. Springer International Publishing. ISBN: 978-3030893071.
Kelley, S.A., et al., 2013. Spatial and temporal trends in pre-caldera Jemez Mountains volcanic and fault activity. Geosphere 9 (1), 614–646. https://doi.org/10.1130/GES00897.
Kumar, Sarkar, P., 2022. A comparison of the AHP and TOPSIS multi-criteria decision-making tools for prioritizing sub-watersheds using morphometric parameters' analysis. Model. Earth Syst. Environ. 8, 3973–3983. https://doi.org/10.1007/s40808-021-01334-x.
Kumar, M., Rana, S., Pant, P.D., Patel, R.C., 2017. Slope stability analysis of Balia Nala landslide, kumaun lesser Himalaya, Nainital, Uttarakhand, India. J. Rock Mech. Geotech. Eng. 9, 150–158. https://doi.org/10.1016/j.jrmge.2016.05.009.
Kumar, A., Singh, S., Pramanik, M., Chaudhary, S., Negi, M.S., 2022. Soil erodibility mapping using watershed prioritization and morphometric parameters in conjunction with WSA, SPR and AHP-TOPSIS models in Mandakini basin, India. Int. J. River Basin Manag. 1–23. https://doi.org/10.1080/15715124.2022.2114485.
Kumar, P., Mittal, H., Kumar, R., 2023. Geohazards: Analysis, Modelling and Forecasting, vol. 53. Springer Nature. ISBN-10: 9819939542.
Malakar, S., Rai, A.K., 2022. Seismicity clusters and vulnerability in the Himalayas by machine learning and integrated MCDM models. Arabian J. Geosci. 15, 1674. https://doi.org/10.1007/s12517-022-10946-1.
Mehta, M., Bhambri, R., Perumal, J., Srivastava, P., Gupta, A.K., 2018. Uttarakhand calamity: a climate revelation in the Bhagirathi River valley Uttarakhand, India, pp. 193–207. https://doi.org/10.1007/978-981-10-3310-0_10.
Meigs, A.J., Burbank, D.W., Beck, R.A., 1995. Middle-late Miocene (> 10 Ma) formation of the main boundary thrust in the western Himalaya. Geology 23 (2), 423–426. https://doi.org/10.1130/0091-7613(1995)023%3C0423:MLMMFO%3E2.3.CO.
Metcalfe, R.P., 1993. Pressure, temperature and time constraints on metamorphism across the main central thrust zone and high Himalayan slab in the Garhwal Himalaya. In: Treloar, P.J., Searle, M.P. (Eds.), Himalayan Tectonics, vol. 74. Geological Society, London, Special Publications, pp. 485–509. https://doi.org/10.1144/gsl.sp.1993.074.01.33.
Miller, V.C., 1953. A Quantitative Geomorphic Study of Drainage Basin Characteristics in the Clinch Mountain Area, Virginia and Tennessee. Tech Rep 3. Columbia University, Department of Geology, ONR, New York, pp. 389–402.
Mueller, J.E., 1968. An introduction to the hydraulic and topographic sinuosity indices. Ann. Assoc. Am. Geogr. 58, 371–385. https://doi.org/10.1111/j.14678306.1968.tb-00650.x.
Mukherjee, S., 2013. Higher Himalaya in the Bhagirathi section (NW Himalaya, India): its structures, backthrusts and extrusion mechanism by both channel flow and critical taper mechanisms. Int. J. Earth Sci. 102, 1851–1870. https://doi.org/10.1007/s00531-012-0861-5.
Mukherjee, S., 2015a. A review on out-of-sequence deformation in the Himalaya. In: Mukherjee, S., Carosi, R., van der Beek, P., Mukherjee, B.K., Robinson, D. (Eds.), Tectonics of the Himalaya, vol. 412. Geological Society, London, pp. 67–109. https://doi.org/10.1144/SP412.13. Special Publications.
Mukherjee, S., 2015b. Atlas of Structural Geology. Springer. ISBN: 978-0128168028.
Patel, A., Singh, M.M., Singh, S.K., Kushwaha, K., Singh, R., 2022. AHP and TOPSIS based sub-watershed prioritization and tectonic analysis of Ami River Basin, Uttar Pradesh. J. Geol. Soc. India 98, 423–430. https://doi.org/10.1007/s12594-022-1995-0.
Patel, A., Ramana Rao, K.V., Rajwade, Y.A., Saxena, C.K., Singh, K., Srivastava, A., 2023. Comparative analysis of MCDA techniques for identifying erosion-prone areas in the Burhanpur watershed in Central India for the purposes of sustainable watershed management. Water 15, 3891. https://doi.org/10.3390/w15223891.
Patidar, A.K., Kothyari, G.C., Kaushik, M., Khanduri, S., 2024. Extraction of tectonic imprints using geospatial techniques: evidence from Mandakini River basin, Uttarakhand, India. J. Mt. Sci. 21, 3720–3738. https://doi.org/10.1007/s11629-023-8339-4.
Pike, R.J., Evans, I.S., Hengl, T., 2009. Chapter 1 geomorphometry: a brief guide, pp. 3–30. https://doi.org/10.1016/S0166-2481(08)00001-9.
Pourghasemi, H.R., Honarmandnejad, F., Rezaei, M., Tarazkar, M.H., Sadhasivam, N., 2021. Prioritization of water erosion–prone sub-WSs using three ensemble methods in Qareaghaj catchment, southern Iran. Environ. Sci. Pollut. Control Ser. 28, 37894–37917. https://doi.org/10.1007/s11356-021-13300-2.
Raha, A., Biswas, M., 2022. Quaternary alluvial fan dynamics of the Jaldhaka basin. J. Mt. Sci. 19, 2160–2179. https://doi.org/10.1007/s11629-021-7005-y.
Raha, A., Biswas, M., Mukherjee, S., 2023. Application of TOPSIS model in active tectonic prioritization: madeira watershed, South America. J. S. Am. Earth Sci. 129, 104502. https://doi.org/10.1016/j.jsames.2023.104502.
Ramírez-Herrera, M.T., 1998. Geomorphic assessment of active tectonics in the Acambay graben, Mexican Volcanic Belt. Earth Surf. Process. Landforms 23, 317–332. https://doi.org/10.1002/(SICI)1096-9837(199804)23:4<317::AID-ESP845>3.3.CO;2-M.
Remondo, J., Oguchi, T., 2009. GIS and SDA applications in geomorphology. Geomorphology 111, 1–3. https://doi.org/10.1016/j.geomorph.2009.04.015.
Roy, S., Das, S., Sengupta, S., 2023. Predicting terrain erosion susceptibility from drainage basin morphometry using ALOS-PALSAR DEM: analysis from PCA-weighted AHP approach in a river system of Eastern India. Environ. Dev. Sustain. 25, 9589–9617. https://doi.org/10.1007/s10668-022-02450-z.
Sadhasivam, N., Bhardwaj, A., Pourghasemi, H.R., Kamaraj, N.P., 2020. Morphometric attributes-based soil erosion susceptibility mapping in Dnyanganga watershed of India using individual and ensemble models. Environ. Earth Sci. 79, 360. https://doi.org/10.1007/s12665-020-09102-3.
Saha, A.K., Gupta, R.P., Arora, M.K., 2002. GIS-Based landslide hazard zonation in the Bhagirathi (Ganga) valley, Himalayas. Int. J. Rem. Sens. 23, 357–369. https://doi.org/10.1080/01431160010014260.
Schumm, S.A., 1956. Evolution of drainage systems and slopes in badlands at Perth Amboy, New Jersey. Bull. Geol. Soc. Am. 67, 597–646. https://doi.org/10.1130/0016-7606(1956)67[597:EODSAS]2.0.CO;2.
Selvan, M.T., Ahmad, S., Rashid, S.M., 2011. Analysis of the Geomorphometric parameters in high altitude glacierised terrain using SRTM DEM data in central Himalaya, India. ARPN J. Sci. Technol. 1, 22–27. http://www.ejournalofscience.org.
Shukla, D.P., Dubey, C.S., Ningreichon, A.S., Singh, R.P., Mishra, B.K., Singh, S.K., 2014. GIS-based morpho-tectonic studies of Alaknanda river basin: a precursor for hazard zonation. Nat. Hazards 71, 1433–1452. https://doi.org/10.1007/s11069-013-0953-y.
Srivastava, V., Srivastava, H.B., Lakhera, R.C., 2009. Information Value Based Spatial Modeling for Landslide Hazard Zonation in the Vicinity of Tons Thrust in Lower.
Strahler, A.N., 1952. Hypsometric (area-altitude) analysis of erosional topography. Geol. Soc. Am. Bull. 63, 1117–1142. https://doi.org/10.1130/0016-7606(1952)63[1117:HAAOET]2.0.CO;2.
Strahler, A.N., 1964. Quantitative geomorphology of drainage basin and channel networks. Handbook Appl. Hydrol. 39–76.
Taloor, A.K., Joshi, L.M., Kotlia, B.S., Alam, A., Kothyari, G.C., Kandregula, R.S., Singh, A.K., Dumka, R.K., 2021. Tectonic imprints of landscape evolution in the Bhilangana and Mandakini basin, Garhwal Himalaya, India: a geospatial approach. Quat. Int. 575–576, 21–36. https://doi.org/10.1016/j.quaint.2020.07.021.
Tewari, N.K., Misra, A.K., Sharma, A., 2019. Assessment of geomorphological and hydrological variations in Bhagirathi River Drainage sub-basin with the help of morphometric studies. J. Taibah Univ. Sci. 13, 1006–1013. https://doi.org/10.1080/16583655.2019.1670888.

Twiss, R.J., Moores, E.M., 2006. Structural Geology, second ed. W. H. Freeman and Company, New York. ISBN: 978-0716749516.
Vanik, N., Shaikh, H., Mukherjee, S., Maurya, D.M., Chamyal, L.S., 2018. Post-Deccan trap stress reorientation under transpression: evidence from fault slip analyses from SW Saurashtra, western India. J. Geodyn. 121, 9–19. https://doi.org/10.1016/j.jog.2018.06.004.
Yin, A., 2006. Cenozoic tectonic evolution of the Himalayan orogen as constrained by along-strike variation of structural geometry, exhumation history, and foreland sedimentation. Earth Sci. Rev. 76, 1–131. https://doi.org/10.1016/j.earscirev.2005.05.004.